Three Phase Piezoelectric Composites for Energy Harvesting Application

Abhishek Mittal

Delft University of Technology

Master Thesis

Three Phase Piezoelectric Composites

By

Abhishek Mittal

to obtain the degree of Master of Science
at the Delft University of Technology, to be defended publicly on 27-March-2018.

Student number: 4502604

Thesis Committee:	Prof. dr. Pim Groen,	TU Delft, supervisor
	Prof. dr. ir. S. van der Zwaag	TU Delft, Chairholder NovAM
	Dr. C.D. (Calvin) Rans	TU Delft

CONTENTS

LIST OF FIGURES

LIST OF TABLES

ABBREVIATIONS

AR	Aspect Ratio
BT	Barium titanate
CNF	Carbon Nanofiber
CNT	Carbon Nanotube
DEP	Dielectrophoresis
EPD	Electrophoretic Deposition
FEM	Finite element Method
GNP	graphene platelets
GLSL	gradient lattice strain layer
HA	hydroxyapatite
KLN	$K_6Li_4Nb_{10}O_{30}$
KN	Potassium Niobate
KNN	Sodium potassium niobate
MWCNTs	Multi wall Carbon nanotube
MEK	methyl ethyl ketone
NG	Nanogenerator
PZT	Lead zirconium titanate
PVDF	Poly vinlydiflouride
PFC	piezoelectric fiber composite
PEGDA	Poly-(ethylene glycol) diacrylate
PMMA	Poly(Methyl methacrylate)
rGO	reduced graphene oxide
SEM	Scanning Electron Microscope
TrFE	Trifluoroethylene
TMPTA	Trimethylolpropane triacrylate

LIST OF SYMBOLS

Symbol	*Description*	*Units*
C	Capacitance	[F/m]
S	Strain	[-]
D	Polarization	[C/m2]
T	Stress	[N/m2]
E	Electric field	[V/m]
d	Piezoelectric charge constant	[C/N] or [m/V]
s	Material compliance	[m2/N]
ε	Dielectric constant (permittivity)	[F/m]
ε_R	Relative Permittivity	[-]
g	Piezoelectric voltage constant	[(Vm/N) or (m/C)]
k	Electromechanical coupling coefficient	[-]
F_{drag}	Drag Force	[N]
η	Viscosity of the matrix	[Pa.s]
ν	Velocity of the particle	m/s
φ	Volume fraction	[-]

1. INTRODUCTION

Piezoelectric materials have now found application in wide range of devices from accelerometers to energy harvesters. They have proven their potential and versatility in aerospace, automotive, electronics and biomedical industry. There is a tremendous increase in the use of low energy device such as biomedical implants, gas sensors and sensors for structural health. The energy source for these devices is mostly conventional batteries that offer limited energy output [1]. Integrating them with energy harvesters can be a much more sustainable solution to power these devices in extreme conditions.

The composites developed in this thesis will have potential application in powering devices with energy consumption below 1 mW. Energy harvesting basically involves utilizing energy from the surrounding environment. Theoretically, this should completely eliminate the batteries in small electrical devices. Such energy harvesters offer advantages such as being environmentally sustainable, applicable in extreme environments, weight reduction, increased lifetime and low maintenance [2, 3].

Typical energy harvesters include thermoelectrics to convert heat into electricity, piezoelectrics to convert mechanical energy into electrical energy or biofuels for extracting chemical energy. The piezoelectric materials can harvest energy from vibrations of a moving vehicle, impact of falling raindrop and as well as from the thermal fluctuations [4, 5].

This chapter will introduce the concepts of piezoelectricity and describe in more detail piezoelectric ceramics and composites. The following sections will lay emphasis on Lead Zirconate Titanate (PZT) and Barium Titanate (BT) based piezoelectric composites, covering the current state of the art. Finally the motivation and research objectives of the thesis project would be presented.

1. 1. Piezoelectricity

Piezoelectricity is coined from the word Piezo which comes from ancient Greek piezein meaning to press or squeeze [6]. The piezoelectric effect involves conversion of mechanical energy into electrical energy or vice versa. Based on the modes energy conversion they are classified into direct and piezoelectric effect. The pair of non-linear constitutive equations describes the direct and inverse piezoelectric effects [7].

$$S = sT + dE \tag{1.1}$$

$$D = dT + \epsilon E \tag{1.2}$$

Where S is strain [-], D is polarization [C/m^2], T is stress [N/m^2], E is electric field [V/m], s is material compliance factor [m^2/N], d is the piezoelectric charge constant [C/N], and ϵ is the dielectric constant or absolute permittivity [F/m].

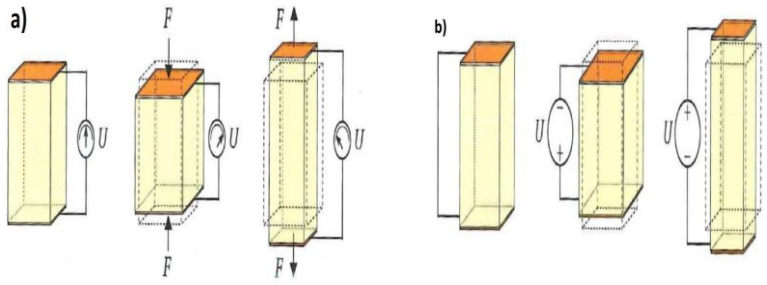

Figure 1: a) Direct Piezoelectric effect b) Inverse piezoelectric Effect [7]

The following equations are also important to calculate the relative permittivity (dielectric constant) [6, 7]:

$$\varepsilon = \varepsilon_r \varepsilon_0 \tag{1.3}$$

$$C = \frac{A\varepsilon_0\varepsilon_r}{t} \tag{1.4}$$

Where ε_r is the relative permittivity (dielectric constant) [-] and ε_0 is the free space permittivity having value: $8.854*10^{-12}$ [F/m]. C is the capacitance of parallel plate configuration having thickness t and area A. The piezoelectric voltage constant can be defined as the electric field generated by a piezoelectric material for a unit stress applied or vice versa [6]. It can be expressed by the following equation:

$$g = \frac{d}{\varepsilon} \text{ [Vm/N or m}^2\text{/C]}, \tag{1.5}$$

where d is piezoelectric charge constant [C/N]

The piezoelectric coupling coefficient (k) is another parameter useful in understanding the piezoelectric properties. The coupling coefficient defines the piezoelectric material ability to convert mechanical energy into electrical energy and vice versa [8]. The value of k is always less than one since the energy conversion is always incomplete [9].

$$k^2 = \frac{\text{mechanical energy converted into electric energy}}{\text{input mechanical energy}} \tag{1.6}$$

The piezoelectric behavior of a material is not always isotropic. Hence it is required to express the constitutive equations in a vector form to take into account the anisotropic behavior of the material. For the piezoelectric charge constant, d_{ij}, and the piezoelectric voltage constant gij, the first index i denotes direction of the electrical quantity while the second index j signifies the mode of mechanical quantity [6].

1. 2. Piezoelectric Ceramics

Ceramics showing piezoelectric properties are polycrystalline in nature and have non-centro-symmetric crystal structure [11]. The ceramics loses its piezoelectricity above a temperature which is called Curie temperature T_c, above which the crystal structure transforms to centro-symmetric crystal structure showing no net dipole moment. Most piezoceramic materials crystallize in the perovskite structure as shown in Figure 2. Barium titanate (BT), lead zirconium titanate (PZT) and alkali niobate are few examples exhibiting such perovskite crystal structure.

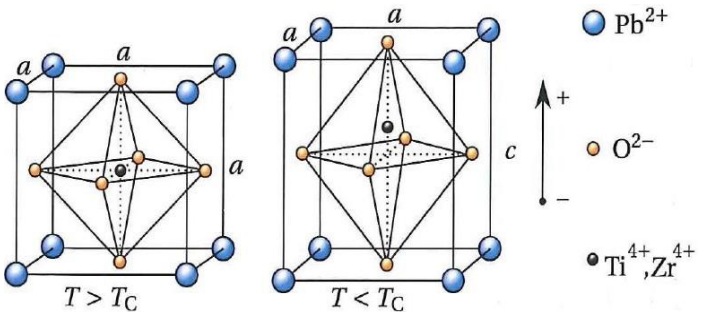

Figure 2: Perovskite crystal structure transition to cubic structure below T_c [10]

1. 3. PZT Composites

PZT ceramics have high piezoelectric charge constants (d_{33}) but have low voltage sensitivity (g_{33}) owing to its high dielectric constant (ε_r) which is generally in the range of 1800-2200. As a result of this PZT ceramics can't be used for sensor applications. Also its processing is difficult due to its brittleness. This leads to the development of PZT polymer based composites having high coupling factor, moderate dielectric composite and better voltage sensitivity along enhanced mechanical properties and flexibility.

The piezocomposite is a system comprising of a polymer matrix phase along with piezoceramic fillers [11]. They give good dielectric and piezoelectric properties of piezoceramic in combination with flexibility and stiffness of polymer phase. Another advantage is the ability to be formed into complex shape without losing its piezoelectricity. The g_{33} of these composites are reported to be as high as $40*10^{-3}$ [Vm/N]. The structured composites can have even higher values of up to $100*10^{-3}$ [Vm/N] [12]. Newnham developed the concept of connectivity which involved various possible ways in which different individual phases are interconnected [12, 13]. The figure below explains the notation convention of piezocomposites. The first index denotes ceramic filler connectivity and the second index signifies polymer matrix connectivity [13, 14].

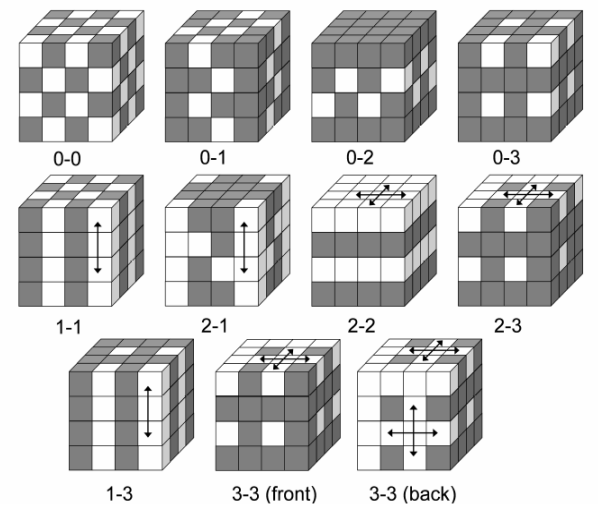

Figure 3: Various types of composites with different connectivity [6]

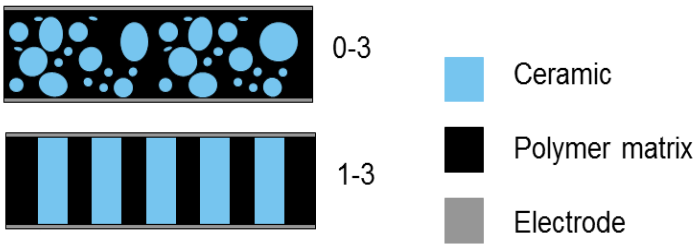

Figure 4: Schematics of random (0-3) and (1-3) composites [17]

Table 1: Dielectric, piezoelectric and mechanical properties of Piezocomposites [21]

Material Type	ε_r	d_{33} [pC/N]	g_{33} [mV.m/N]	Young's Modulus [GPa]	References
0-3 PZT (70%) – Epoxy	100	45	51	49.6	[19]
0-3 PZT (40%) – Epoxy	21	8	43	29	[17]
1-3 PZT(10%) – Epoxy	11	7.5	77	8.7	[17]
1-3 PZT (60%) – Epoxy	45	17	43	42.8	[17]
0-3 PZT (70%) – PVDF	105	25	27		[38]
0-3 PZT (50%) – PU	48	30	71		[39]
0-3 PZT (50%) – PA	68	28	47		[41]
0-3 PZT (40%) - LCT	30	13	49		[42]
0-3 BNBT (30%) – P(VDF-TrFE)	21	14	75	33.7	[16]
0-3 PZT (30%) – Zn ionomer	9	5	63		[33]
0-3 PZT (30%) - EMMA	8	2	28		[33]
1-3 BNKLT (75%) – Epoxy	734	195	30	[-]	[13]
1-3 KNNL(10%) – Epoxy	13	13	118	11.7	[19]

Out of various different modes of connectivity the composites based on 0-3 and 1-3 connectivity have mostly been studied till date. The ceramic phase in a 1-3 composite is ideally connected in one direction like a continuous fiber while the polymer phase is connected in all three directions. They offer excellent electrical properties in the direction of particle alignment. They have certain limitations such as fabrication complexity, labor intensive, high production cost and prone to fracture [12, 17]. The 0-3 composites offer much more flexibility than the 1-3 composites due to uniform dispersion of the ceramic filler in the polymer matrix. Also cost of production and

fabrication complexity is much less. But these composites offer low piezoelectric and dielectric properties due to limited partide connectivity and greater dielectric mismatch between the ceramic and polymer phase. This is reported as the main cause of unwanted electric field distribution in the composites [16]. A brief comparison of various 0-3 and 1-3 piezocomposites properties are tabulated below.

1. 4. BT Composites

The section gives an overview on the various developments in $BaTiO_3$ (BT) based piezoelectric composites and investigate into the current state of art. The overview focuses in a greater detail into the processing methodology and electrical properties of the composites. Furthermore a brief critical assessment is presented on the feasibility of these composites from the application point of view.

R. Popielarz et al. did an investigation on Batio3/polymer composites in 2001 where they measured the dielectric properties over wide range of frequency and temperature [17]. This was the first reported study on dielectric properties of such composites over wide frequency range (100 Hz to 10 GHz). Measurements were also done in microwave frequency range due to measurement technique being developed for the solid films [28]. BT as the ferroelectric filler was used having an average particle size of 1μm. Three different types of polymer were used: Trimethylolpropane triacrylate (TMPTA), Poly-(ethylene glycol) diacrylate (PEGDA) and 1, 14-tetradecanedioldimethacrylate (TDDMA).The study showed that the dielectric properties are highly dependent on the type of polymer matrix. Dielectric constant for polar polymers increased with the increase in frequency at low frequencies range but there was no further increase in gigahertz frequency range. It was also found that the dielectric losses were increased significantly with the rise in polarity of the polymer matrix.

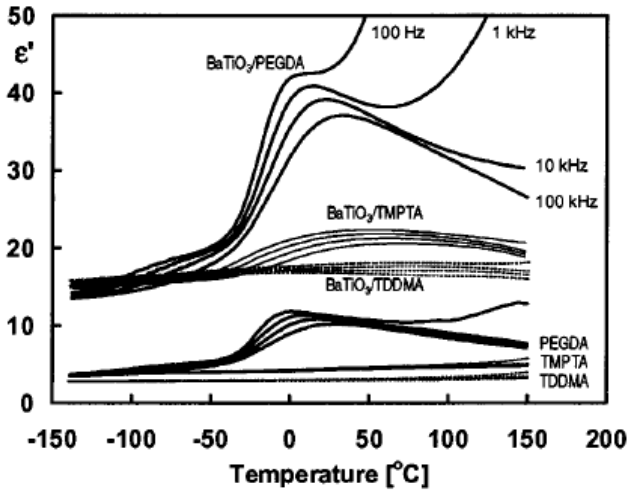

Figure 5: Temperature dependence of dielectric constant of 30% BT/polymer composites [17]

The maximum dielectric constant of 40 was observed for a BT/PEGDA composite at 25°C and 100 Hz (Fig. 5). This polymer matrix shows a large variation in dielectric constant with varying temperature and frequency which makes very unreliable for any practical application. On the other hand BT/TDDMA composite, the least polar polymer matrix, has a very low dielectric constant variation making it feasible for the industrial application [17].

Another such investigation was carried out on 0-3 PVDF-TrFE/ BT composites by a group of researchers from EPFL [17]. The composites of 60 vol% Bati03 were prepared by solvent casting and compression molding. The effect of various processing conditions on the dielectric and piezoelectric properties of the composites were investigated. The solvent cast composites were prepared by first dissolving P(VDF-TrFE) in methyl ethyl ketone (MEK) at 60°C in an oil bath. The powders were then slowly added and placed under ultrasound bath for deagglomeration of the powders [20]. The solution was finally casted on glass and the solvent was evaporated in vacuum. The compression molded composites were prepared by standard compression molding procedure in a TP50 hydraulic press.

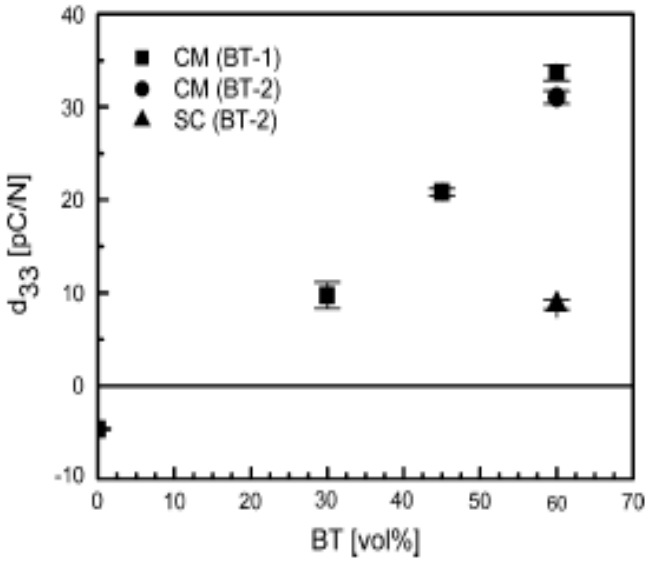

Figure 6: Piezoelectric Coefficient of CM and SC composites Vs $BaTio_3$ vol% [20]

The study reported d_{33} values as high as 34 pC/N for 60 Vol% $BaTio_3$ as can be seen in the above figure. The d_{33} of the compression molded composites increased linearly from -5pC/N (pure polymer). The solvent casted composites showed much lower properties than the compression molded ones.

1-3 fiber based piezoelectric composites show excellent piezoelectric properties at the cost of increased difficulty in fabrication [21]. Also its very difficult and complex to fabricate 1-3 composite having ceramic phase in the order of 100 μm [21]. To develop a piezoelectric composite having good properties of 1-3 and ease of fabrication of 0-3 studies were conducted by L. F. Chen et al. on BT whiskers based PVDF composites [22]. Since the active phase (whiskers) is not self connecting it's still technically has 0-3 connectivity but has the high anisotropy of a 1-3 composite (fig. 7).

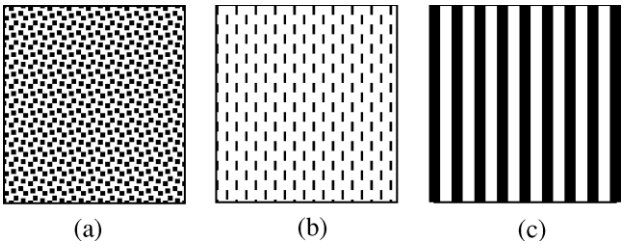

Figure 7: Schematics of piezoelectric composites with the active phases a) 0-3 (particle) b) whiskers C) 1-3 fibers [22]

The average length and diameter of the used whiskers were 3 μm and 0.3 μm. The whisker alignment was achieved by hot pressing of a precursor fiber, comprising of PVDF solution and BT

whisker, in a die to form the composite. These fibers can be placed in 0° or 90° direction to achieve the required alignment (fig. 7). The whiskers are highly aligned along the axis of the fibers due to extrusion and drawing in polymer solution wet spinning (fig. 8). The drawing ratio here governs the degree of alignment of whiskers [21].

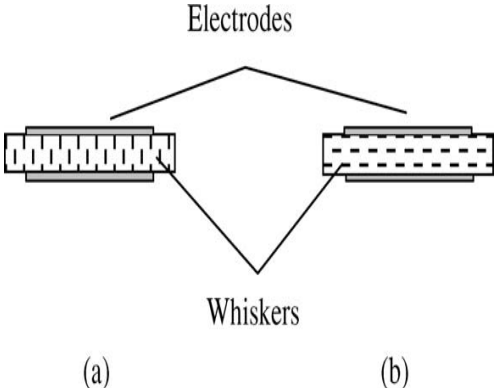

Figure 8: whisker orientation: (a) normal to electrode surface b) Parallel to electrode surface [21]

The reported dielectric constant of the whisker composites is higher than the 0-3 powder based composites. ε_r for a normal and parallel 30% PVDF composite was 90.72 and 44.40 respectively. While for the powder based PVDF composite ε_r was just 23.89. The d_{33} values of normal and parallel specimen were 13.7 pC/N and 10.6 pC/N respectively, significantly higher than the powder based composites. The increase in electrical properties was explained by the concept of percolation threshold that can cause increase in the connected passage density leading to higher degree of polarisation [21, 22].

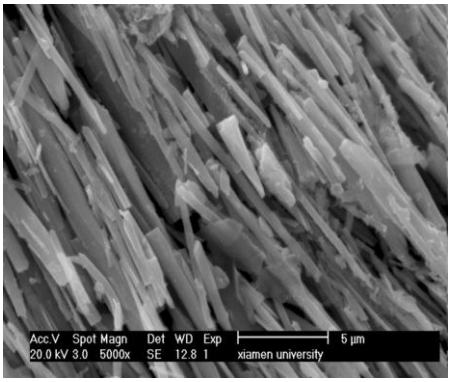

Figure 9: SEM of parallel composite after organics removal, showing whisker alignment [21]

Another study by researchers from Arizona State University deals in synthesis of a novel piezoelectric fiber composite (PFC) where the multifunctional structural fiber comprises of SiC fiber core and BT piezoelectric shell [23]**.** The major motivation of this work was develop a composite with embedded electrode that can be a sensor or actuator along with a load carrying structure. The SiC fibers were coated with BT powder by Electrophoretic Deposition(EPD) process having an average coated particle size 150 nm[24] (fig. 10).

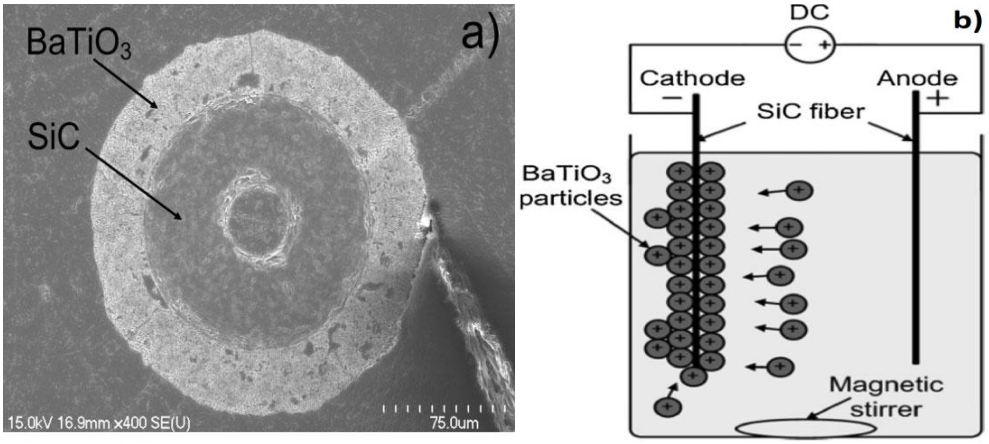

Figure 10: a) Cross-section of Active Structural Fiber (ASF) b) EPD process [23]

The authors reported a maximum effective piezoelectric coupling value (d_{31}) of 34.08 pm/V at 0.67 aspect ratio. The electrochemical coupling was reported to increase linearly with the increase in the fiber aspect ratio. The fabrication process seems to be feasible for industrial application owing to its fast and low cost technique [23].

Somewhat similar studies were also conducted by Bowland et al. at university of Florida to develop multifunctional barium titanate coated carbon fiber for sensing and energy harvesting application [24]. A two step hydrothermal process was incorporated for synthesizing $BaTio_3$ film on carbon fibers. The researchers first synthesized an array TiO_2 nanowires that were aligned vertically. The hydrothermal process then converts TiO_2 nanowires to Ba and modifies the morphology to nanowire film (fig. 11).

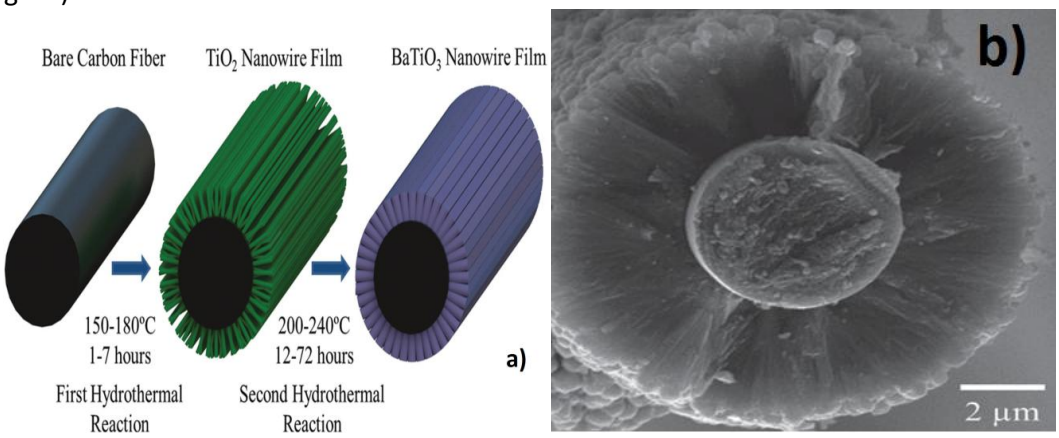

Figure 11: a) Two - Step hydrothermal Process b) Cross-section structured fiber having $BaTio_3$ nanofilm surrounding carbon fiber core [24]

The study reported average d_{33} and d_{31} values of 31.6 ± 14.5 pm/V and -5.4 ± 3.2 pm/V. The authors successfully demonstrated the application of such structured fiber for vibrational energy harvesting operational at low frequencies. Woongchul Choi et al. investigated the effect of increasing aspect ratio of $BaTio_3$ nanowires on its dielectric and piezoelectric properties [25]**.** Here also the $BaTio_3$ nanowires were synthesised by a twp step hydrothermal process as described in the previous study. The diameter of nanowires synthesised were in the range of few 100 nm. The nanocomposite film was prepared by solvent casting process.

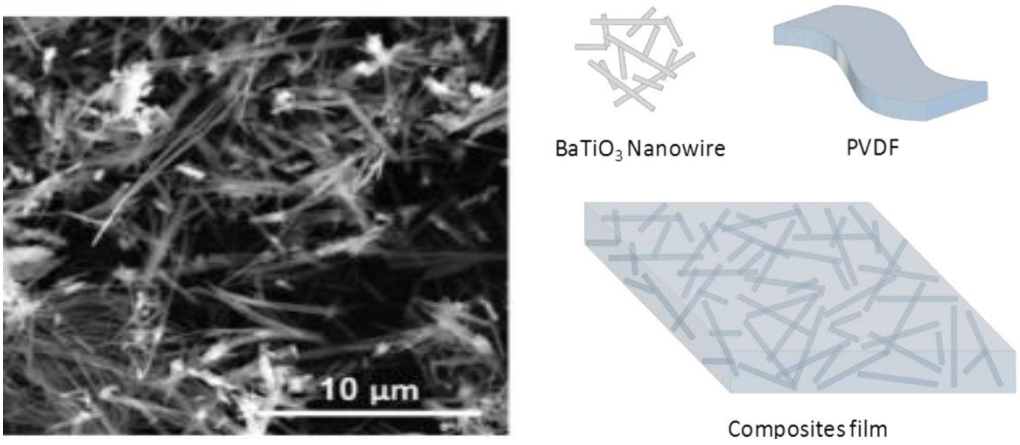

Figure 12: a) SEM of $BaTio_3$ nanowires b) $BaTio_3$ nanowire based composite thin films [26]

The maximum dielectric constant reported in this study was up to 64 with 50 vol% $BaTio_3$ nanowires having an AR of 18. There was hence an improvement by 800% as compared to composites having $BaTio_3$ nanoparticles. The properties improved with the increase in BT vol%. The study also reported saturation of piezoelectric coefficient (d_{33}) after a poling time of 10 min (fig. 13).

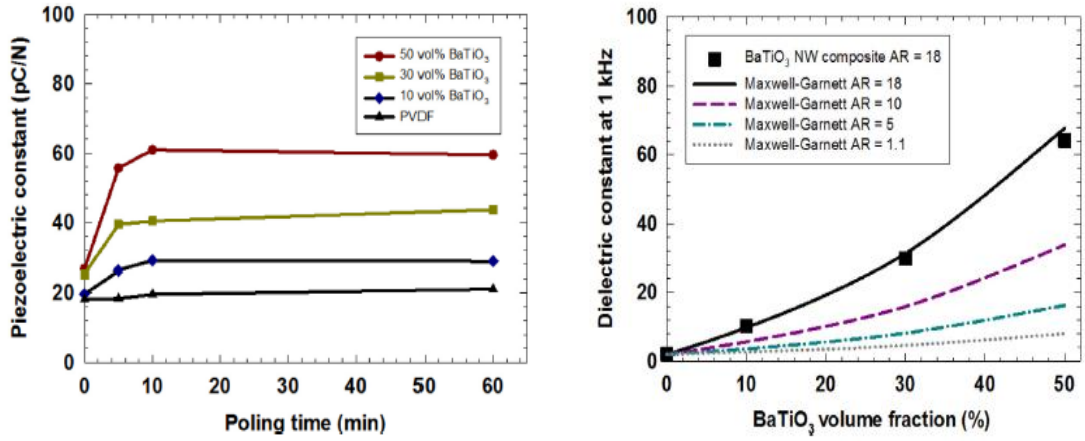

Figure 13: a) d_{33} Vs Poling Time b) Dielectric constant Vs BT **Vol%. Experimental values compared to Maxwell Garnet Model at various AR [26]**

Recently in one particular study the effect of addition of BT nanoparticles in piezoelectric fiber composites (PZT/Epoxy) was investigated [27]. The objective was to decrease the dielectric mismatch between PZT fiber and epoxy leading to increase in active electric field in PZT fibers causing a significant improvement in d_{33} and actuation properties [28]. Barium titanate nanoparticles were treated with dopamine for surface modification so as to achieve tight adhesion with epoxy. Thin film composite of BT/epoxy were first fabricated and then PFCs synthesized by viscous polymer process [26]. Sintered stacks of PZT were filled with BT loaded epoxy. Vol% of PZT fibers was kept at 75.8 %(fig. 14).

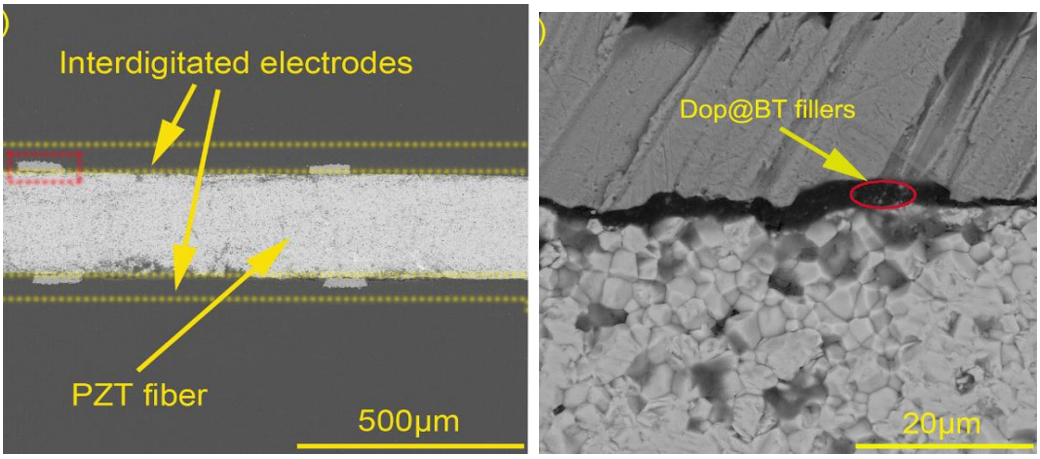

Figure 14: The cross sectional micrographs of PFC (a) parallel to PZT fibers (b) BT/ epoxy layer between copper electrode and PZT fiber [27]

The study reported an increase in free strain and effective d_{33} at first but subsequently declined with further addition BT in epoxy. The free strain and d_{33} reached a maximum value of 1820 ppm and 455 pm/V at 6 wt% BT. The results from this study proved the models about variation in applied electric field in piezoelectric fibbers influenced by dielectric constant of the epoxy. The addition of BT nanoparticle in PFCs seems to be an effective solution to decrease poling and actuation voltages [27].

1. 5. Dielectrophoresis

The connectivity between the different phases is a crucial parameter that influences the physical and electrical properties of piezoelectric composites. 0-3, 1-3 and 3-3 are the most common connectivities being used in making a diphasic composite. Only the 1-3 composites show superior piezoelectric properties as a result of its anisotropy. Fabricating 1-3 composites require sophisticated techniques. This chapter will mostly talk about such fabrication techniques developed so far to structure the ceramic filler in a polymer based composite.

1-3 structured composites can be fabricated by various methods such as injection molding, dice and fill, lost mold, tape casing and laser cutting. However, all these methods are expensive and labor intensive [28]. To reduce fabrication costs and retain flexibility of 0-3 composites a novel fabrication technique was developed by di-electrophoretic processing (DEP). This basically involves aligning of ceramic particles in polymer matrix into a chain like structure resulting in a quasi 1-3 piezoelectric composite [28, 29]. DEP involves polarization of ceramic filler in the presence on electric field. This causes mutual attraction force between particles and their orientation towards the applied electric field to from chain like structure [30]. The electric field is removed after the curing of polymer matrix, locking the particles in their chain formation.

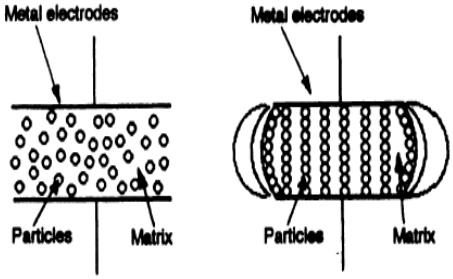

Figure 15: Particle aligning by DEP in piezoelectric composites [17]

Both James et al. [19] and Van Den Ende et al. have demonstrated excellent piezoelectric and dielectric properties by particle aligning from DEP route. This can be seen clearly in fig. 16 below where the d_{33} values for DEP structured composites(PZT/Epoxy) are considerably higher than the random composite at similar volume fraction of PZT partides(φ) [17]. It has also been reported that the flexural modulus of DEP structured composites is higher than the random composites. This was attributed to the loss in polymer chains mobility due to ceramic chains formed via DEP [19].

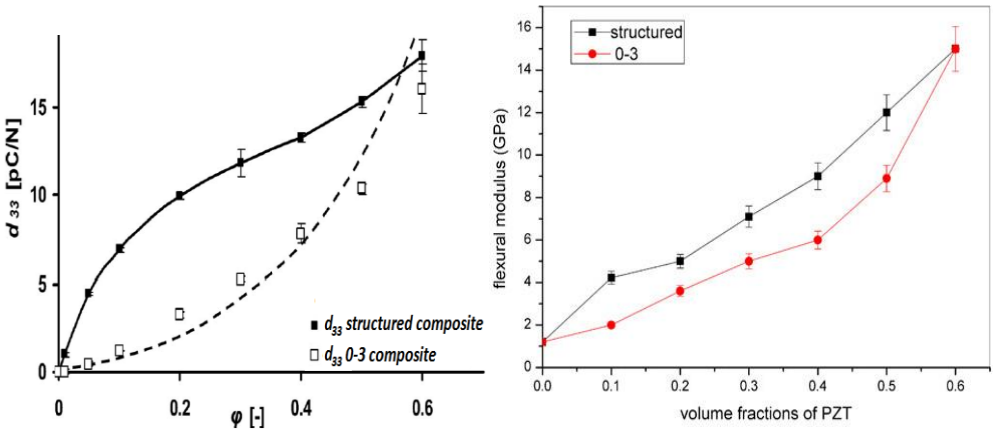

Figure 16: a) d_{33} values for 0-3 and DEP Structured PZT-Epoxy composites [14] b) Flexural modulus variation of random and DEP structures PZT/Epoxy composite with PZT vol% [16].

The degree of particle alignment can be quantified by using an order parameter $\overline{P_2}$ [31] which can be expressed as:

$$\overline{P_2} = \overline{(3\mathrm{Cos}^2\beta\text{-}1)/2} \tag{1.6}$$

Where β is the angle between the major axis of fitted ellipses over the ceramic particle and electric field direction [17]. $\overline{P_2} = 0$ for completely isotropic phase (random composites) and $\overline{P_2} = 1$ for structures composites having complete particle alignment .The particle alignment can be influenced by various factors such as ceramic particle size, dielectric constant, electric field voltage and frequency. The driving force (time averaged), F_{DEP} that is responsible for the mutual attraction of the particles towards the electric field can be expressed by the following equation [17]:

$$F_{DEP} = 2\pi\varepsilon_1 r^3 \mathrm{Re}[K^*(\omega)]\nabla E^2_{RMS} \tag{1.7}$$

Here ε_1 is the permittivity of matrix, ω is the angular frequency, r is the particle radius and E_{RMS} is applied electric field root mean square value. $K^*(\omega)$ is a complex Clausius Mossotti function which influences the particle attraction or repulsion to the strong electric field region. The constant has to be positive to achieve chain like particle alignment since $K^*(\omega) > 0$ implies permittivity of ceramic

particle is more than that of matrix [19]. It depends on the permittivities and conductivities of ceramic and matrix respectively, which can be expressed as follows:

$$K^* = \frac{\varepsilon_2^* - \varepsilon_1^* - j\frac{\sigma_2 - \sigma_1}{\omega}}{\varepsilon_2^* + 2\varepsilon_1^* - j\frac{\sigma_2 + 2\sigma_1}{\omega}} \quad (1.8)$$

Where σ_1, σ_2 are the conductivities of ceramic & matrix and ε_1^*, ε_2^* are the permittivities of ceramic and matrix. As we can see from the above equation, the frequency of the applied electric field influences the sign and magnitude of this function. For every material system there exists an optimum frequency at which the phase angle of Lissajous plots is at its maximum value so as to ensure that there is lowest possible dielectric loss from the polymer matrix [30].

Another important factor that affects the particle alignment is viscosity of the polymer matrix [17]. The drag force experienced by a particle increases with the increase in matrix viscosity, η. This drag force, F_{drag} can be easily calculated by using the Stokes's law for flows having low Reynolds's no.:

$$F_{drag} = 6\pi\eta\nu r \quad (1.9)$$

Here r is the particle radius and ν is the particle velocity. The velocity in turn can be computed by the following equation:

$$F_{DEP} - F_{drag} = 0 \quad (1.10)$$

The viscosity of the thermoset polymer matrix increases with time due to crosslinking, which is a time dependent process. This means the particle velocity would decrease and delay particle alignment. Hence how fast the particle alignment is also a crucial parameter in deciding the piezoelectrical properties. Thermal noise and gravitational force are some other parameters that influence the particle flow in a fluid. But they are not considered for the particle alignment if the polymer matrix curing is at low temperature and there is negligible particle sedimentation [17].

1. 6. Three Phase Piezoelectric Composites

Two phase piezoelectric composites have limitations such low piezoelectric and dielectric properties due to the presence of non-conductive polymer matrix [34, 35]. This causes problems in polarization of the ceramic materials [36]. To overcome these limitations 3 phase piezoelectric composites were developed and researchers started experimenting with different conductive fillers [37]. Majority of such 3 phase composites have 0-0-3 connectivity pattern, where the piezoelectric ceramic and conductive filler are not interconnected while the polymer phase is linked in all three directions. Some 3 phase composites were also reported to be developed by foaming of polymer matrix having 1-3-0, 3-1-0 & 3-2-0 connectivity [14].

Percolation threshold was reported to be an important parameter that influenced the properties of such 3 phase composites [38]. This chapter will talk in greater detail about various 3 phase piezoelectric composites being developed focusing specifically on the fabrication route, type of filler and its electrical properties.

Use of conductive fillers in a polymer matrix has been reported by several researchers [39-42]. Each study showed significant improvement in the conductivity of the matrix due to the presence of conductive fillers. Sa-Gong e al [43] experimented with various third conductive phase such as carbon, silicon or germanium to improve the poling efficiency of piezoelectric composites. Park et al.

[44] added CNTs in BT based nanocomposites which served as conductive functional materials. It reported higher output voltages due to formation of complex mixture of BT with CNT networks. Ma and wang reported an increase in the conductivity of a PMN-PZT/Epoxy 0-3 composite with the increase in volume fraction of carbon nanotubes (CNT) [45]. This increase was attributed to the formation of conductive pathways due to percolation effect. The percolation threshold in these composites was found around 1g CNTs per 100g epoxy Polyamide 11/PZT/CNT nanocomposites were demonstrated to achieve percolation threshold at very low CNTs concentration (0.35 Vol %) with a highest d_{33} value at 0.2 vol% CNTs [46]. The composite was made by an extrusion process which involves introducing conductive fillers into the matrix in molten state.

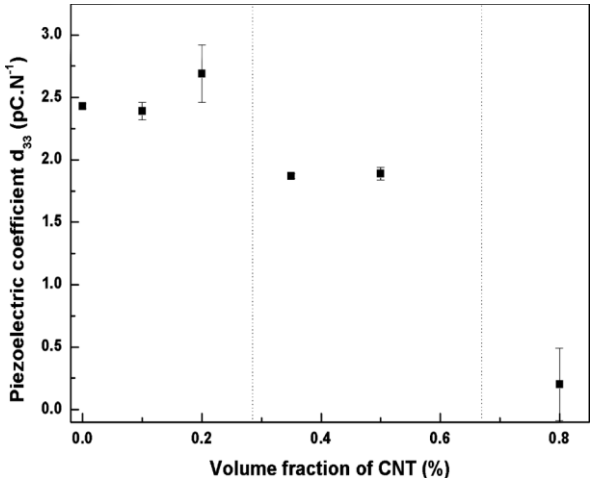

Figure 17: a) SEM image of 3 phase PA11/30%PZT/0.2%CNT composite b) Variation d_{33} with CNT volume fraction [46].

Multiwall carbon nanotubes (MWCNTs) have also been extensively investigated for inclusion in polymer matrix [47, 48]. They show high electrical conductivity due ease of electron transportation along the tube length and its unidirectional nature. In a recent study MWCNT/PZT/epoxy composite fabricated showed d_{33} value of 18.87 pC/N at 30 vol% PZT and 6 vol% MWCNT [49]. The samples were fabricated by sol-gel & hot moulding method and poled by contactless (corona) poling technique to prevent dielectric breakdown due to the presence conductive fillers [50, 51].

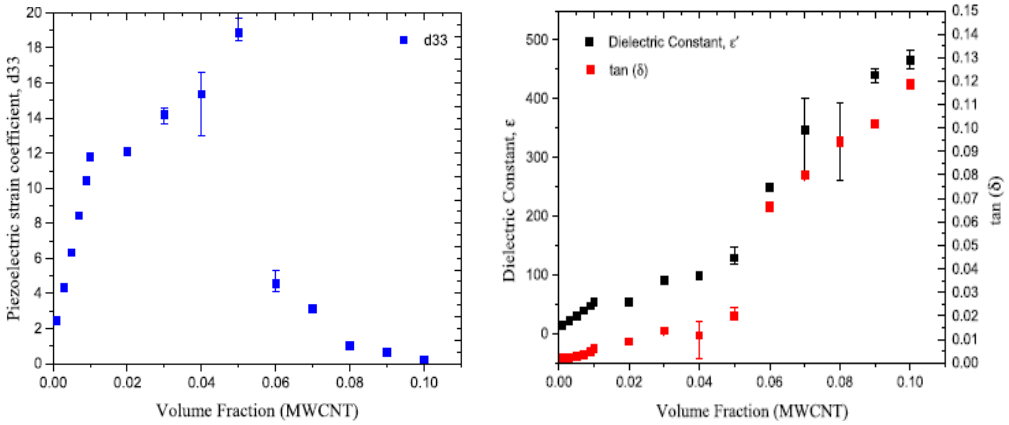

Figure 18: a) Variation of d_{33} with MWCNT volume fraction measured at 110 Hz and 0.25 N b) Variation of dielectric constant and tan δ with volume fraction of MWCNT [49]

3 phase piezoelectric composites comprising of PZT, carbon black and epoxy were demonstrated to show superior damping loss factors then two phase composites [50]. The maximum damping loss

factor reported was 0.08 for 0.51 wt. % carbon black and 69.7 wt. % PZT. The enhanced damping values were due to the flow of generated current through carbon black partides. Jise Mao et al. reported synthesis of asphalt based PZT composite dope with carbon black and demonstrated maximum piezoelectric strain factor and dielectric constant of 75.74 pC/N and 154.89 respectively at 0.3 vol% carbon black/80% vol PZT [51]. The further increase in carbon black concentration caused decrease in the piezoelectric activity due to high resultant electrical conductivity. The composite was prepared by compression moulding technique under a pressure of 90 MPa for 1 min at 120°C.

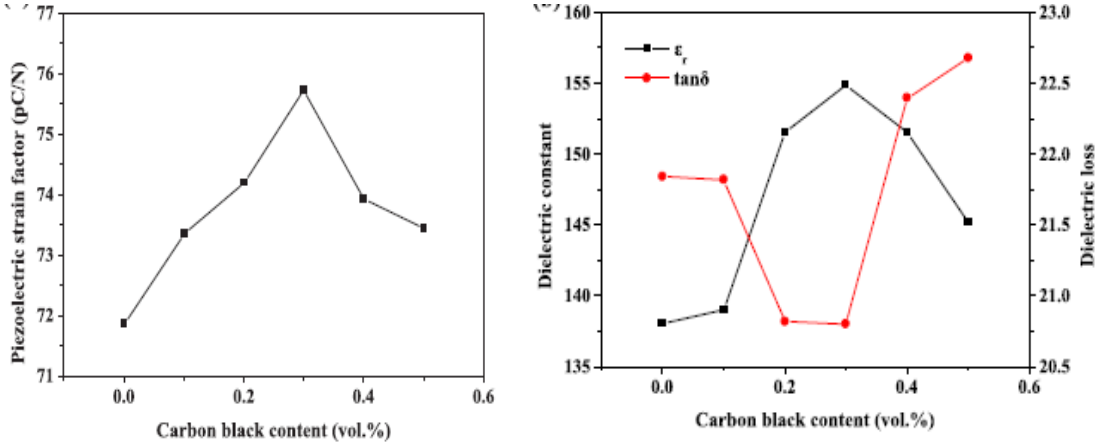

Figure 19: a) Variation of d_{33} of carbon black/PZT/asphalt composite with carbon black vol% b) Dielectric constant & Dielctric loss variation with carbon black vol% [51]

A low cost alternative to CNTs and MWNTs are graphene platelets as conductive filler materials for piezoelectric composites [52, 53]. One study reported use of graphene platelets (GnPs) in a PZT/epoxy composites showing tremendous improvement in piezoelectric and electro-mechanical properties [51]. Percolation threshold reported was as low as 1-2 vol%. D_{33} values were found to be as high as 9.8 pC/N at 0.25 wt% GnP. The composite was prepared by conventional film casting technique having 70% by weight concentration of PZT [65].Recently, a PMMA based nanocomposite with BT and reduced graphene oxide (rGO) was investigated for its dielectrical properties [56]. The study reported a maximum value of 8.5 at 0.15 wt% rGO and 5 wt% BT where a further increase in rGO concentration causes sharp decrease in the dielectric constant [57]. Thick films of high aspect ratio rGO platelets nanocomposite were fabricated via solution method and casted by Doctor's Blade technique having a film thickness of 0.5 mm.

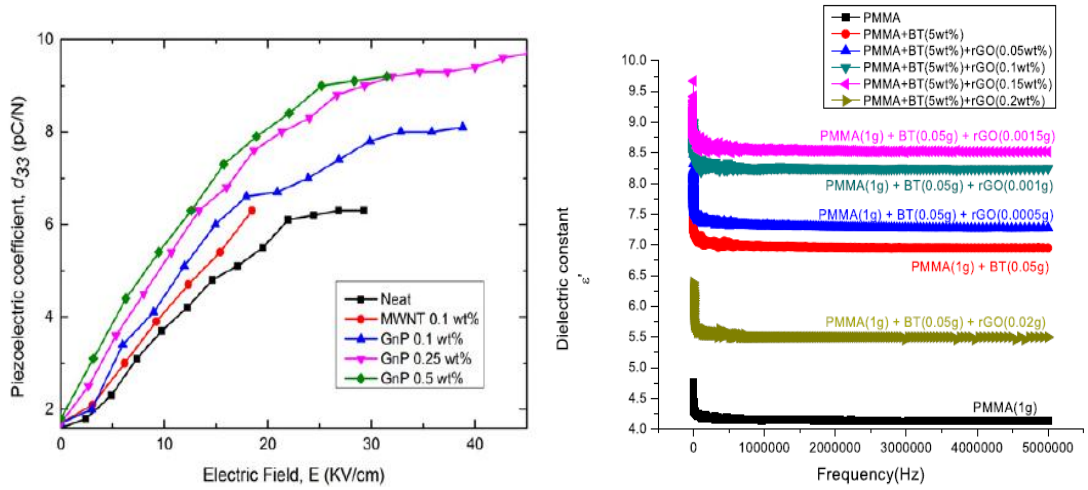

Figure 20: a) Piezoelectric activity variation vs. Poling field of GnP/PZT/Epoxy piezocomposites for different GnP concentration [51] b) Dielectric response of rGO/BT/PMMA nanocomposite in the frequency range of 100 Hz – 5 MHz [56].

Just like in 2 phase piezoelectric composites, particle size and distribution in the polymer matrix are critical factors that determine the piezoelectric properties of a composite. Choi et al. investigated the particle size effects of BT in BT/Ni/PMMA composites which were synthesized by a two-step mixing and hot molding process. They reported increase in dielectric constant and decrease in the percolation threshold of Ni with the increase in particle size of BT from 80nm to 1μm [58]. The particle size effects would be explored in depth in the upcoming chapters. Other than carbon based conductive fillers, Al particles have also been investigated owing to their low density, high electrical conductivity and relatively low cost. Banerjee et al. investigated the dielectric and piezoelectric properties of PZT/Al/Epoxy composites which were fabricated by sol-gel and hot moulding technique [59]. Significant improvement in properties was reported due to the presence of conductive Al fillers. The particle size and distribution of the filler in the epoxy matrix played a key role in the properties [59-62]. The maximum d_{33} value reported was 6 pC/N at 70 vol% PZT and 20% Al micro sized particles [62]. Al/PZT/Portland cement was demonstrated to show even better electrical properties reporting a maximum d_{33} and dielectric constant value of 8.1 pC/N and 80 respectively at 70 vol% PZT and 20% Al [63]. The composite was fabricated by conventional cold pressing technique in a hydraulic compression machine at about 100 MPa.

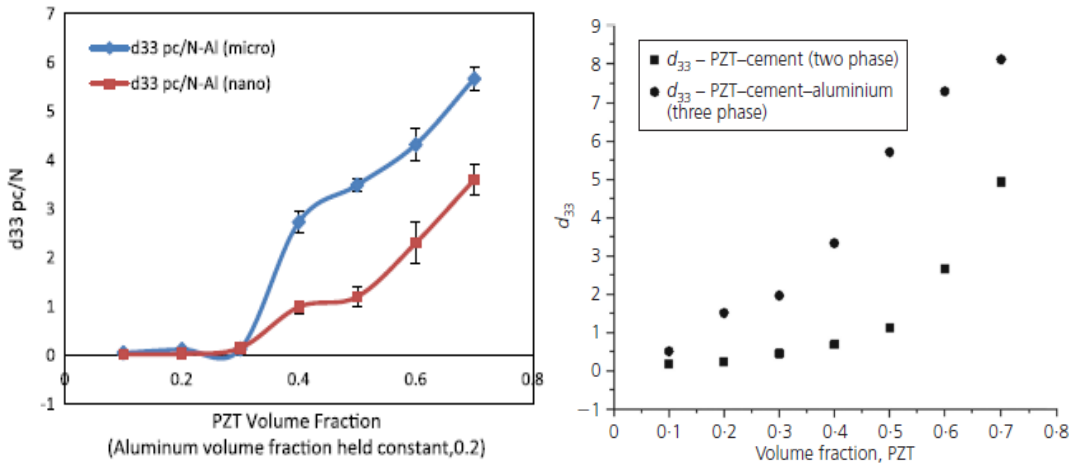

Figure 21: a) d_{33} variation with PZT volume fraction in Al/PZT/Epoxy composite [59] b) d_{33} vs. volume fraction of PZT in both cement based 2 phase and 3 phase composite [63].

1. 7. Barium Titanate Particle Size Effects

$BaTiO_3$ (BT) is considered to be one of the alternatives for lead free piezoelectric ceramics since its highly characterized and have been used in piezoelectric applications [64, 65]. BT is ferroelectric having tetragonal phase at room temperature. Above Curie temperature of 130°C it is paraelectric having cubic phase [66]. Ferroelectric properties are reported to be influenced by particle size at nanoscale [67, 68]. This chapter will talk in greater detail about the grain size and particle size effects with a greater focus on its crystal structure and optimum particle size.

The ratio of lattice constant (c/a) for BT if found to vary with particle size and transition from tetragonal to cubic with decreasing size [69-71]. This transition is reported to be in range of 10 – 100 nm depending a lot on particle synthesis conditions and defect structure such as the presence of Ba^{2+} ions [82]. This decrease in c/a with particle size is known as ferroelectric size effect in numerous studies due to the fact that spontaneous polarization is dependent on the tetragonality of the crystal lattice [80, 83-85]. The relationship between c/a (tetragonality) and spontaneous polarization P_s is given by the following equation [76, 77]:

$$Ps \sim (c/a)^{0.5} \tag{5.1}$$

The particle dielectric constant $\varepsilon_{r,par}$ is also size dependent [70,71] and affects in turn the particle polarization in a composite. This can be explained by means of space charge effects at the ceramic/polymer interface. Its shown to be related to dielectric constant of the composite $\varepsilon_{r,compo}$ by the Lichtenecker equation [78] :

$$\log \varepsilon_{r,compo} = \nu_{par} Log \varepsilon_{r,par} + \nu_{polymer} \log \varepsilon_{r,polymer} \tag{5.2}$$

Here ν_{par}, $\nu_{polymer}$ are volume fractions of particle and polymer respectively. Goswami [79] reasoned the small dielectric constant of powdered BT (>2μm) due to surface defect layer having low dielectric constant on the surface. The mean electric field acting on particles in a composite responsible for spontaneous polarization is given by Furukawa [80]:

$$E_{par} = \frac{3\varepsilon_{r,polymer}}{2\,\varepsilon_{r,polymer} + \varepsilon_{r,par} + \nu_{par}(\varepsilon_{r,polymer} - \varepsilon_{r,par})} E_{app} \tag{5.3}$$

here E_{app} is the applied electric field.

Until now there are very few experimental studies been conducted on investigating directly the ferroelectricity of different BT particle size especially at the nanometer scale. The majority of studies discusses about the effect of particle size on the crystal structure. T. Hoshina et al. investigated experimentally and theoretically the dielectric properties of $BaTiO_3$ fine particles ranging from 20-430 nm [81]. The particles were synthesized by a two-step decomposition technique of barium titanyl oxalate for defect and impurity free BT particles [82-86]. The maximum dielectric permittivity reported was around 5000 at 140nm.

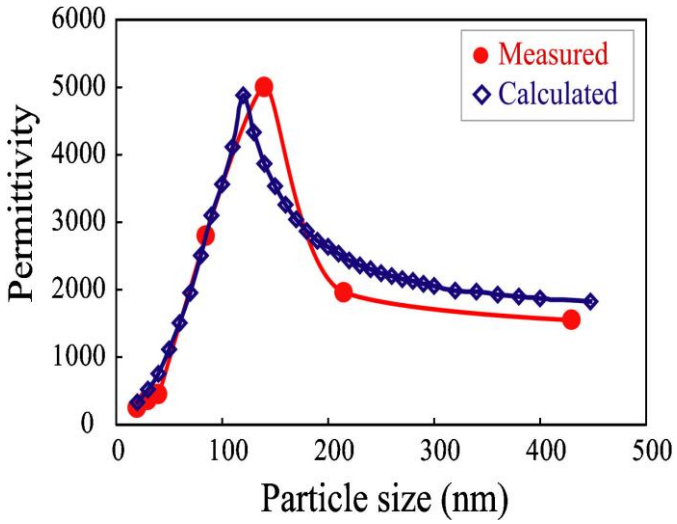

Figure 22: Dielectric permittivity variation with BT particle size [82]

The results were supported by a new particle composite structure model [82] where in a BT nanoparticle is assumed to have three sections: "(1) inner tetragonal core (2) gradient lattice strain layer (GLSL) (3) surface cubic layer". GLSL is the static phase transitional layer from tetragonal phase to cubic phase. The lattice ratio c/a of the inner tetragonal core was found to be independent of the particle size and only the volume fraction of inner tetragonal core changed. So the size effect only influenced the volume fraction of these regions [84]. This is in contrast with the earlier reported work on c/a of BaTiO3 particles [87-89]. The model deduced the constant thickness (10-15 nm) of surface cubic layer invariant of the particle size. This implied that the ferroelectricity should disappear below the critical size of 20-30 nm due to the loss of tetragonal core below this point.

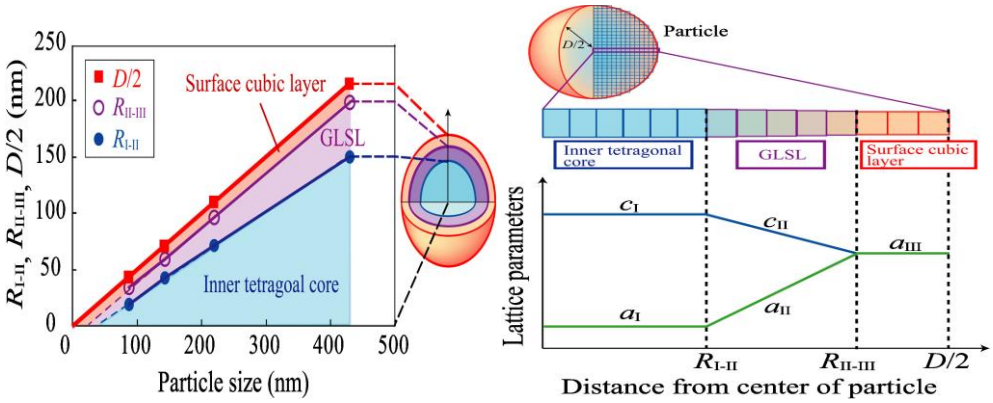

Figure 23: a) Inner tetragonal core thickness variation with particle size b) Overview of proposed particle composite model [84]

S. Wada et al. reported very high dielectric constant value of 15000 at a partide size of 70nm where the particle processing conditions were quite different from the previous study [90]. The dielectric properties of partides were measured by novel technique involving suspensions [91, 92]. The figure below shows the variation in a-axis and c-axis due to particle size effect suggesting phase transition from tetragonal to cubic at 150 nm [93].

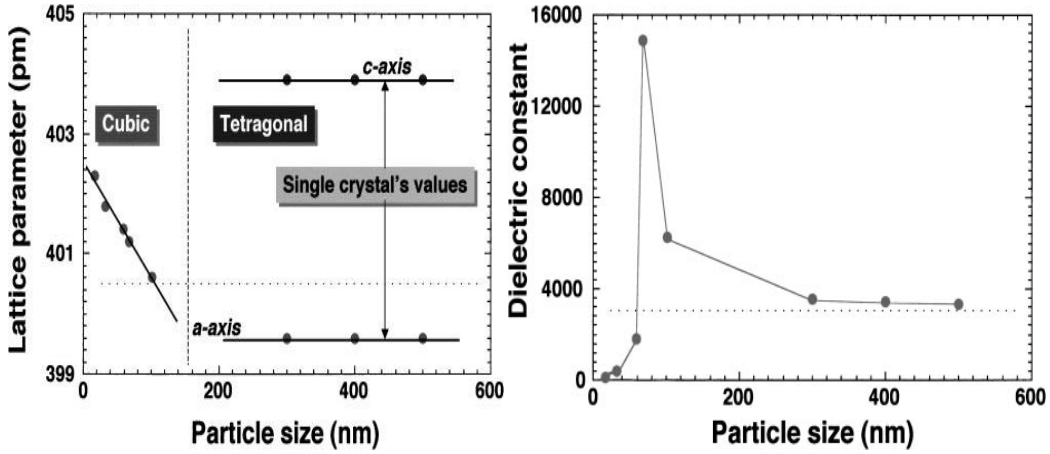

Figure 24: a) lattice parameter variation with particle size b) dielectric constant variation with the particle size [103]

Recently investigations were done to explore experimentally size effects of BT particles in a polymer matrix wherein ferroelectric polarization of the ceramic partides were directly measured by novel technique [94]. Adams et al. measured directly instantaneous ferroelectric polarization of BT particles (10nm – 0.8 μm) in a cyanoresin CR-M matrix to explore the particle size effect in the piezoelectric composite. The novel measurement technique is a modified version of PUND (positive switching pulse-up/negative switching pulse-down) method [95]. Spin coating fabrication technique was used here to make thin film composites. It was reported that the electric field required achieving a certain level of polarization increases with decreasing partide size. The electric field varies from 3 – 35 V μm^{-1} to achieve instantaneous composite polarization of 1 $\mu C\ cm^{-2}$ [95].

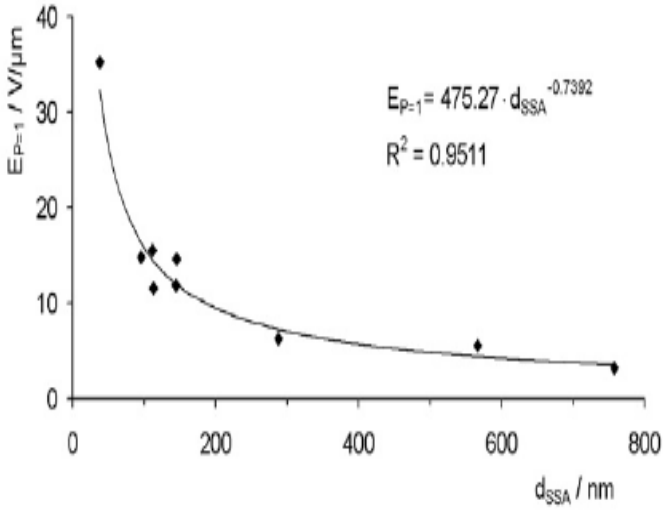

Figure 25: Variation of $E_{p=1}$ with particle diameter. $E_{p=1}$ is the value of electric field required to get composite polarization of 1 $\mu C\ cm^{-2}$. [105]

1. 8. Motivation and Thesis Objective

Composites consisting of particles of PZT or its lead free alternatives in a polymer matrix have been shown to have promising properties for the application as sensor materials or for energy harvesting systems. Improvement of properties can be achieved by orienting the particles into chains inside the polymer by a process called electrophoresis. However, the dielectric mismatch between the piezoelectric particles, which have a high dielectric constant, and the polymer matrix, which typically have low dielectric constants make the poling during the final step in making a piezoelectric composite difficult.

The research question which is addressed in this work is to find ways to lower the dielectric mismatch by the addition of extra (nano) particles in the composite to screen the mismatch in dielectric constants. To achieve this 3 phase composites are suggested in which the 3rd phase is barium titanate which is available in various particle sizes. The relative dielectric constant of this material is dependent on the particle size of barium titanate. The "ideal" microstructure which would give the improved properties is schematically shown in figure 26.

The research was planned as follows:

- To investigate the effect of the particle size of barium titanate, BT, on the dielectric constant 2 phase composites have been made at relative high volume loading of 50% in an epoxy and a PDMS polymer.
- For reference 2 phase PZT composites have been made.
- Hereafter, three phase composites are investigated containing 10 vol. % PZT and a varying amount of coarse grained (3 μm) BT. Random composites and quasi 1-3 composites, made by dielectrophoresis, have been made.
- Finally, three phase composites are made using nanoparticles of barium titanate.

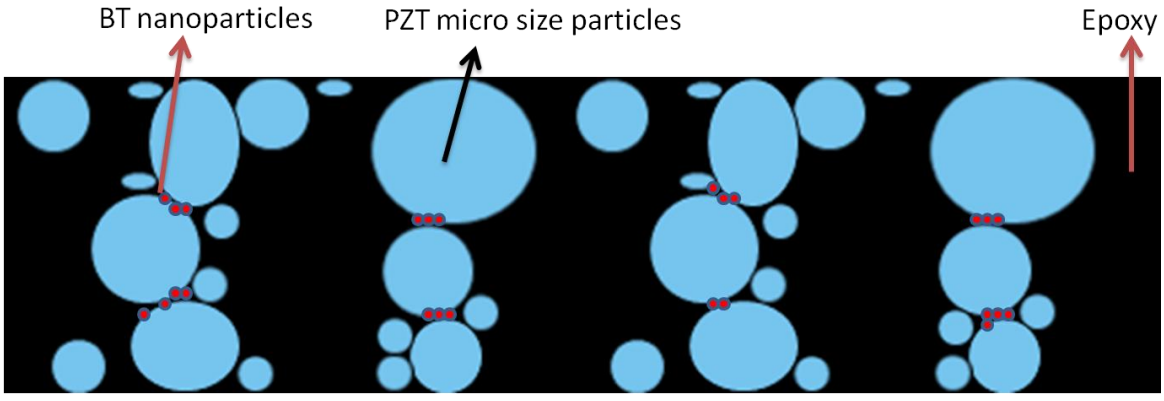

Figure 26: Ideal BT/PZT particle structuring

2. EXPERIMENTAL TECHNIQUES

This chapter will mainly cover the fabrication process and various characterisation techniques performed throughout the thesis project. A brief overview on the selection of ceramic filler and polymer matrix is also presented.

2. 1. Materials

The ceramic powder or filler used in this thesis project was Lead Zirconate Titanate ceramic powder (PZT5A4), from Morgan Electroceramics, UK and Barium Titanate (BT) from KCM, Japan. The main aim in this project is demonstrate a proof of concept for a 3 phase composite with enhanced piezoelectric properties. So for such a study the above mentioned ceramic filler were best fit since they were well characterised and easily available. Also high dielectric constant ceramic filler was also a requirement which BT easily satisfies.

For polymer matrix, a two component epoxy system (Epotek 302-3M, Epoxy Technology Inc., Billerica, MA, USA) based on diglycidyl ether of bisphenol – A (DGEBA) resin and poly (oxypropyl)-diamine (POPD) multi-functional aliphatic amine curing agent. Both components are colorless liquids at room temperature. The T_g of the Epoxy polymer system cured at 50°C for 3 hr and post cured at 100°C for 1 hr is 60°C [106]. It has a dielectric constant of 5.26 at 1 kHz and room temperature, making it a desired option for dielectrophoresis (DEP).

A two component polydimethylsiloxane (PDMS) (SYLGARD 184, Dow Corning Corporation, MI, USA) is also used in this study. It consists of part A as the silicone elastomers base and part B as the silicone curing agent. Both the components are colourless liquids at room temperature. The viscosity of the cured resin is 3.5 Pa.s at room temperature. It has considerably much longer processing window then the epoxy polymer system, which is about 1.5 hr at 25°C. It has a dielectric constant of 3.3 at 1 kHz and has the T_g at -120°C [107].

2. 2. Ceramics Powder Preparation

The PZT5A4 were calcined at 1150°C for 1 hour to get a single phase crystalline material. The powder received from calcination was heavily agglomerated, so it was dry-milled to micron size particle range in a jar by using 5 mm zirconium balls for 3 hours. This powder was hand milled to break apart partially sintered powder. It was then sieved with a mesh size of 63µm and dried at 150°C to remove the moisture. The BT nanoparticles were not processed since the calcination process can drastically affect the particles size.

2. 3. Composite Fabrication

The piezoelectric composite fabrication typically involves a series of steps. First, the ceramic filler and polymer part-A (resin) is mixed in a planetary mixer (Speed mixer DAC 150 FVZ, Hauschild) at 2500 rpm for 5 mins. After this, the polymer part-B (hardener) is added and mixed again at 2500 rpm for 5 mins. This composite mixture is then degassed in a vacuum chamber for 15-30 mins depending

upon the polymer system and is then mixed again at 2500 rpm for 5 mins. The mixing is done to negate the effects of sedimentation during the degassing process. The mixture is poured into a steel mould having Teflon sheets of 1mm thickness and circular cut-outs of diameter 15 mm. Two layers of Al sheet of thickness 50 um was placed on both the sides acting as electrodes during the Dielectrophoresis (DEP) process. It was ensured that a uniform pressure is applied to get flat samples. Additional Teflon sheets of thickness 1mm were added as insulating layers to avoid shirt circuiting of the Al electrodes with the steel plates.

During the DEP process, AC voltage of 1kV/mm and 1 kHz is applied via a function generator (Agilent 33210A) and high voltage amplifier (Radiant Technologies Inc., T6000HVA – 2). The set frequency of 1 kHz for epoxy system gives highest phase angle and hence least electric field losses. The phase angle, peak to peak voltage, and frequency were monitored via an oscilloscope (Agilent, DSO-x 2004 A). The composites were kept on hot plate at 60°C for 3 hrs to cure during the DEP procedure. The random composites were fabricated by curing them at 60°C for 3 hrs without the application of electric field. The fig. 27 illustrates the entire fabrication procedure.

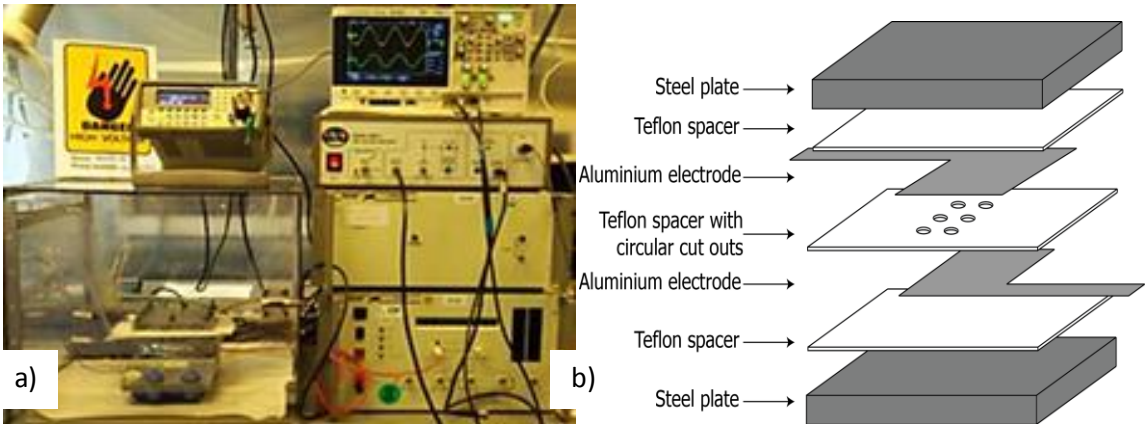

Figure 27: a) Dielectrophoresis Setup b) Schematics of the Steel/Teflon Mould used [96, 97]

2. 4. Electroding & Poling

After curing of the piezoelectric composites, the surface is grinded with silicon carbide paper of grit size 1000. This is done to have a better adhesion of the gold electrode layer to the surface of the composites. The composites are then left for post-curing for 1hr a 100°C to remove any moisture. After this a gold layer of 25 nm thickness is deposited on either surfaces of the composite in a sputtering system Quorum Q300TD. For poling, a DC voltage of 10 kV/mm was applied in a silicon oil bath at 110°C for duration of 30 mins. This was then cooled down to the room temperature in the presence of the electric field. The composites were then covered with Al sheets to remove the excess surface charges and left to age for 24 hrs before doing measurements for its piezoelectric properties.

(a) (b)

Figure 28: a) Gold sputtering Setup b) Poling Setup

2. 5. Characterization

The crystal lattice structure and phase identification of BT powder were evaluated by X-ray Diffraction (XRD) patterns using Cu Kα radiation having a wavelength of 1.789 A° (Rigaku, MiniFlex600). The angular range was set to 10 °- 90°, using step width of 0.02° and scan speed of 0.05 secs/step. These conditions allowed having a good quality of diffraction patterns for the obtained BT ceramic filler, necessary for determining the tetragonality and crystal lattice structure. The different diffraction patterns were first indexed with the available PDF cards of various BT phases and then post-processed in origin.

Figure 29: Rigaku MiniFlex600 X-ray Diffractometer

The capacitance of composites, before and after poling, was measured using an Agilent 4263B LCR meter (parallel plate capacitor) at 1 V and 1 kHz. The piezoelectric charge constant, d_{33} is measured with a Berlin court type PM300 d_{33} meter at 10N & 110 Hz. A SEM (JEOL, JSM-7500F) is used to observe the microstructure of the BT nanopartides and 2 phase & 3 phase piezoelectric composites.

(a) (b)

Figure 30: (a) LCR meter (b) Berlin court d_{33} meter.

The microstructure of the cross-section of random and structures campsites were observed via Field Emission Scanning Electron Microscope (SEM) [JEOL JSM -7500F, Japan]. The samples are always polished with a series of diamond paste and a thin layer of gold (10nm) is deposited to avoid charge buildup during SEM imaging process. These charge buildups can drastically deteriorate the image formation since it directly influences the incoming electron beam. An optical microscope (Keyence, VHX 2000, Osaka, Japan) is also used to evaluate the ceramic alignment and agglomeration in the structured piezoelectric composites.

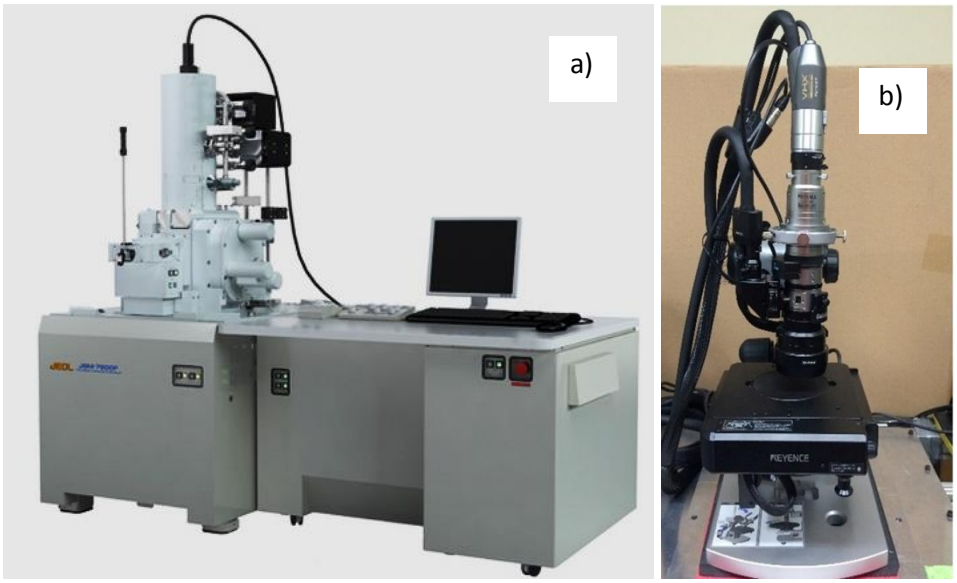

Figure 31: a) JEOL Scanning Electron Microscope b) Keyence Optical microscope

3. Barium Titanate Characterisation

This chapter will talk mainly about the characterisation of the BT nanoparticles of various sizes. The aim here is to see the variation in the particle morphology and crystal structure with the particle size. First, the particle size analysis is discussed followed by the XRD of nanoparticles.

3. 1. Particle Size analysis

The particle size analysis of BT nanoparticles was done by SEM. The micrographs were analysed using ImageJ to determine the particle size for various samples of nanoparticles. The average particle sizes were found in the range of 30 – 150 nm. It can also be noticed that the coarseness of the nanoparticles varies with the particle size as seen in the fig. 32. Also it can be observed from the SEM images that the 30nm and 60nm BT ceramic have a spherical geometry while the 100nm and 150nm BT ceramics have an irregular morphology.

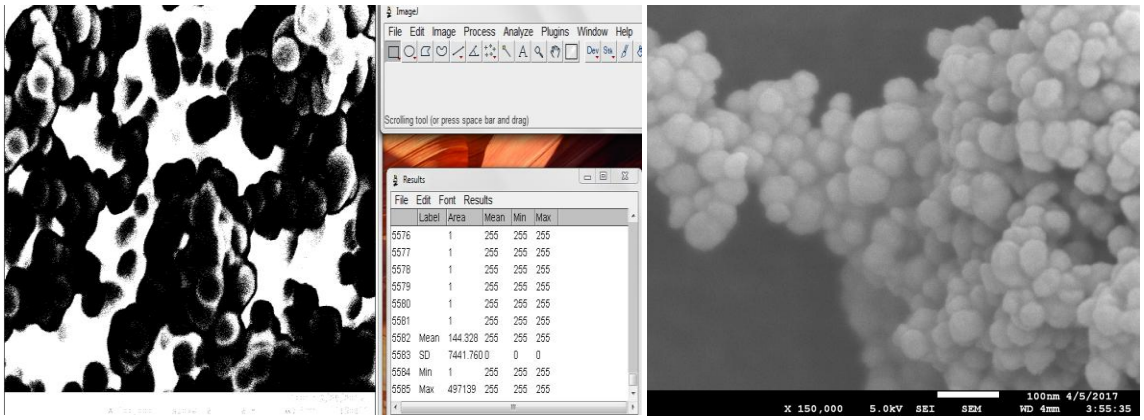

a) Analysis of SEM micrographs in ImageJ *b) 30RF [32±7 nm]*

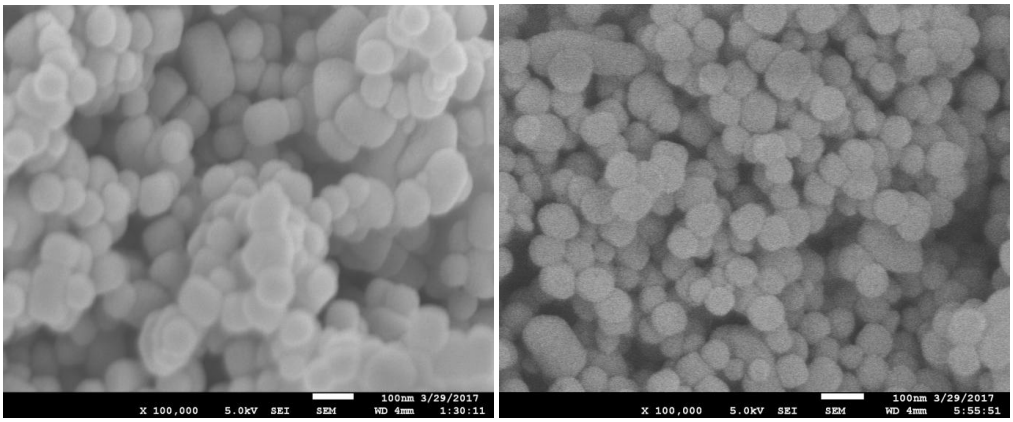

c) TODAA60R [64±6nm] *d) 100R [95 ± 8 nm]*

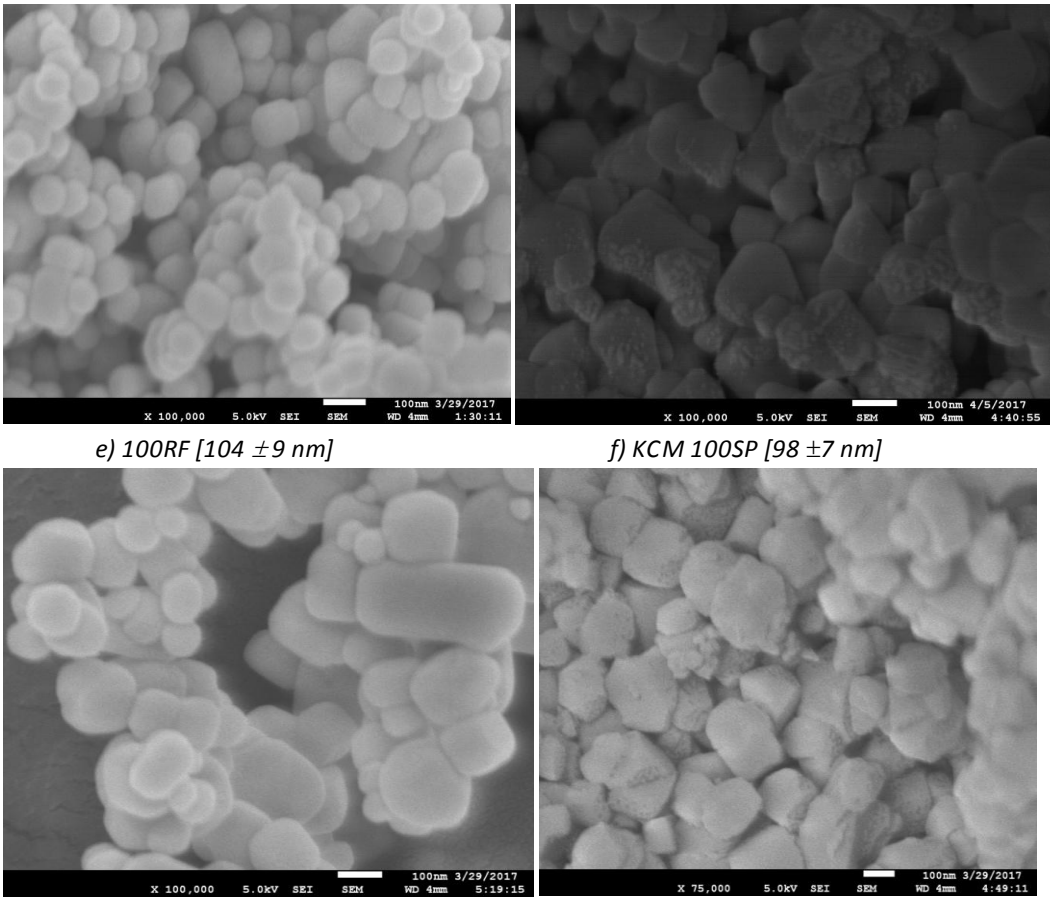

e) 100RF [104 ±9 nm] *f) KCM 100SP [98 ±7 nm]*

g) TODA 155RK [147 ±9 nm] *h) KCM150SP [154 ±7 nm]*

Figure 32: BT nanoparticle particle size analysis in SEM. Micrographs were used to determine average particle size of the BT nanoparticles from different manufacturers.

3. 2. XRD

The crystal structure of nanoparticles of varying particle sizes were determined through the XRD patterns using Cu Ka radiation. The main aim was to find the particle size threshold at which the crystal structure is cubic and how the particle size influences the tetragonality of the BT lattice structure. The fig. 33 shows the diffraction patterns of various samples of nanoparticles. It was found that the BT nanoparticle of average particle size 30nm to be cubic as indicated by the narrow peak at $2\theta \sim 45°$.

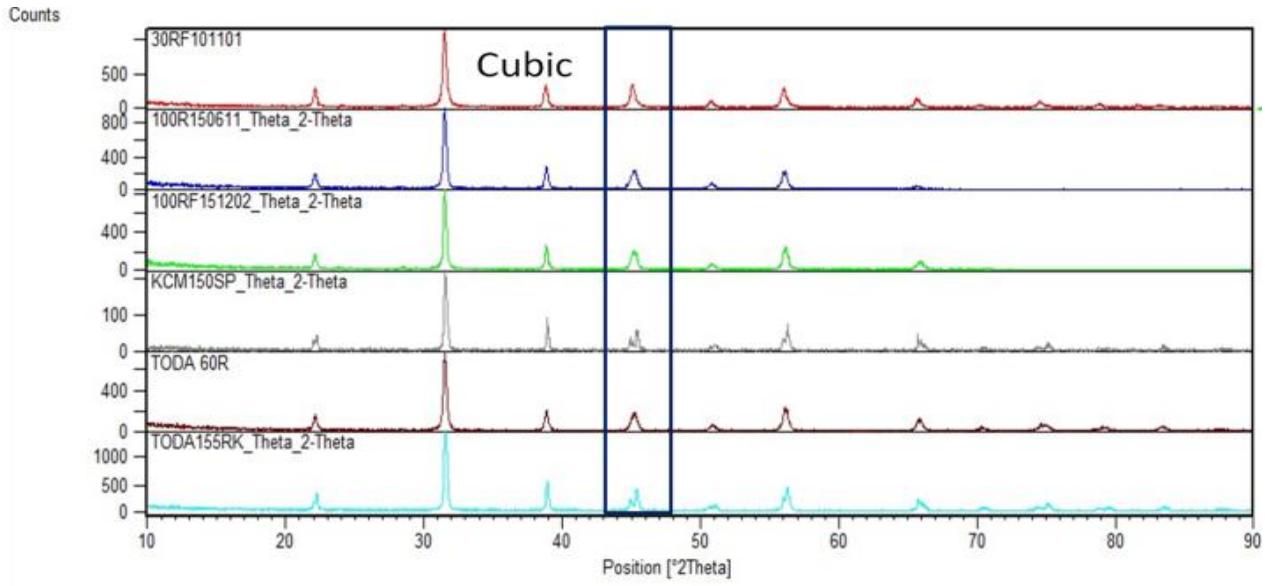

Figure 33: XRD pattern of BT nanoparticles

Using these XRD patterns, the lattice constants were determined and c/a ratio was deduced to get the crystal structure tetragonality. It was found that the c/a ratio or the tetragonality increased with the increase in the particle size of BT nanoparticles. The c/a ratio for the 30nm BT particles was found to be 1 indicating a cubic lattice structure.

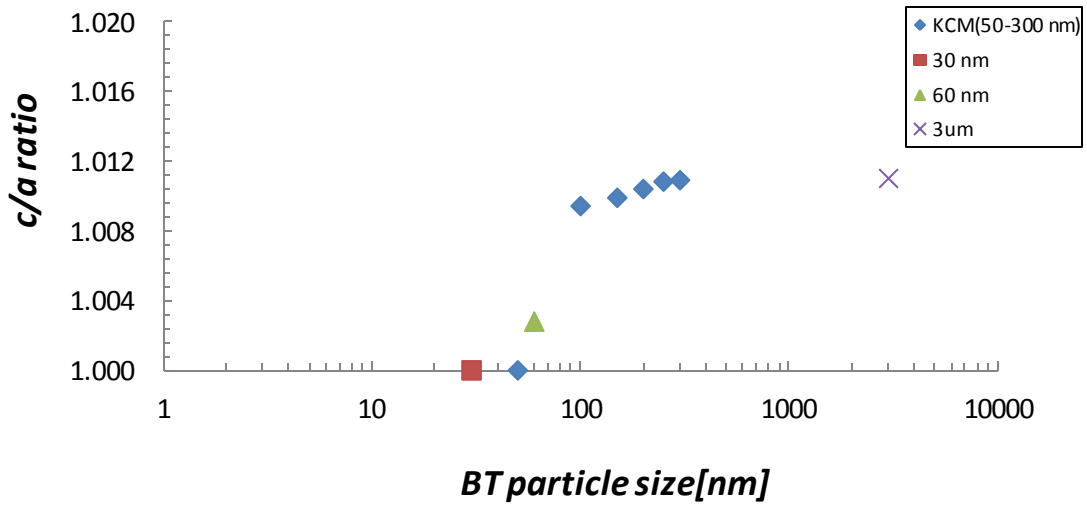

Figure 34: c/a ratio calculated from XRD patterns

4. TWO PHASE COMPOSITES

This chapter will cover all the experimental studies pertaining to two phase piezoelectric composites synthesised. The fabrication route and characterisation results will be discussed. First the PZT composites with epoxy as polymer matrix are synthesised as a reference. This is then followed by synthesis of BT composites with both epoxy and PDMS as polymer matrix.

4. 1. BT/Polymer Composites

The BT based polymer composites were synthesised to characterise its dielectric properties. Four batches of two phase composites were made having different BT volume fraction and polymer matrix. This is described in detail in table 2. In all the batches of two phase composites, BT of particle size 50,100,150,200,250, and 300 nm are used.

Table 2: Two Phase BT composites specifications

Batch No.	BT Vol%	Polymer Matrix	BT particle Size (nm)						
			1	2	3	4	5	6	7
A	40vol%	PDMS	50	100	150	200	250	300	3000
B	50vol%	PDMS	50	100	150	200	250	300	3000
C	40vol%	Epoxy	50	100	150	200	250	300	3000
D	50vol%	Epoxy	50	100	150	200	250	300	3000

The synthesis procedure of these two phase composites involves the following steps. First, the polymer resin (Part A) is mixed with the hardener (Part B) in a speed-mixer for 5 mins at 2500 rpm. This mixture is immediately set for de-airing process in a degassing chamber for removing the entrapped air. For PDMS polymer system degassing is done for 30 mins while for the Epoxy system it's done for 15 mins. BT ceramic filler is then added to the degassed mixture and mixed in a speed-mixer at 3000 rpm for 5 mins. The rpm is kept at much higher level during mixing due to the volume fraction of BT ceramic fillers used. The resultant thick suspension is placed into Teflon moulds and set for curing overnight. It is ensured that they are clamped as tightly as possible by means of Al plates so as to get a flat surface. After curing of the composites, they are demoulded and polished using a grinding paper. PDMS based composites were not polished due to their brittle nature and presence of small cracks. After the composites are dried in an oven for 1hr at 100°C, gold electrodes were sputtered on both sides. Since the composites were synthesised just to characterize its dielectric properties, no poling was done. The SEM results are shown in fig. 35. The cross-section of composite samples was polished and gold sputtered before being characterised. The SEM images show the even distribution of BT ceramic filler in the polymer matrix. It can also be observed that the air entrapments are in acceptable level.

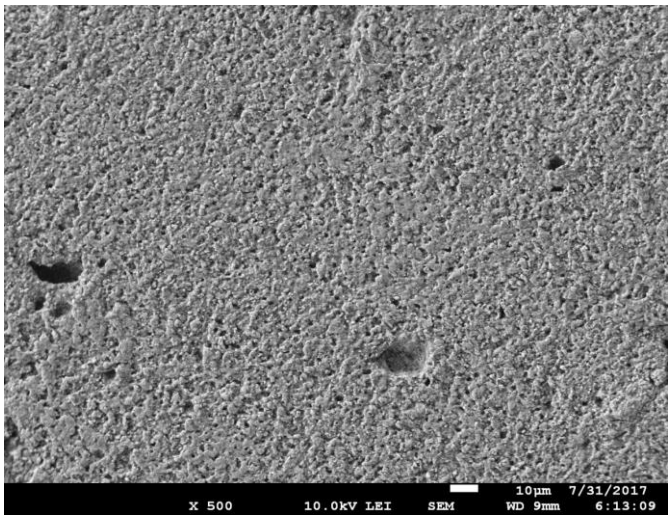

Figure 35: SEM micrograph of 50% BT (150nm)/PDMS composite at 500x

The results of dielectric properties of the two phase composites are shown in the fig. 36 and fig. 37. It was found that the dielectric constant of the composites increases with the BT particle size till a certain threshold. The dielectric constant was found to be highest for composites with BT of particle size 300nm. This trend was observed for all the four batches of composites irrespective of the BT volume fraction and polymer matrix. It can be concluded than that the dielectric constant of BT particles itself is dependent on its particle size as mentioned in previous theoretical studies by Hoshina and Wada [94, 96].

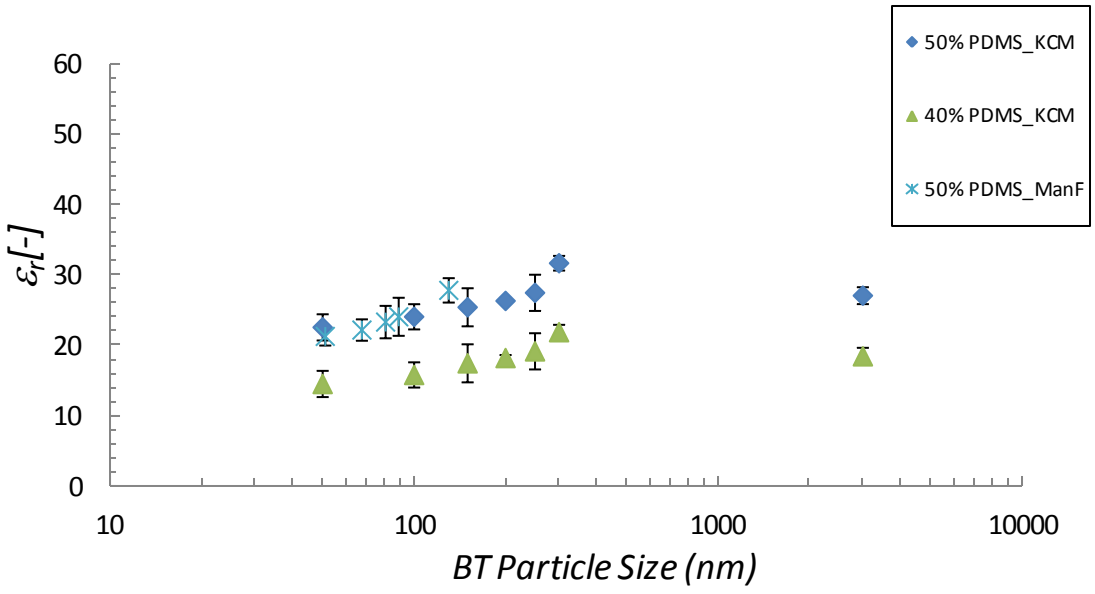

Figure 36: Dielectric properties of BT/PDMS composites

As expected, the dielectric constants of 50 vol% BT composites are higher than that of the 40 vol% BT composites. Also the dielectric constants for the Epoxy based composites are much higher than the PDMS based composites. This is due to higher dielectric constant of Epoxy (ε_r = 5.26) than the PDMS (ε_r = 3.3) polymer system.

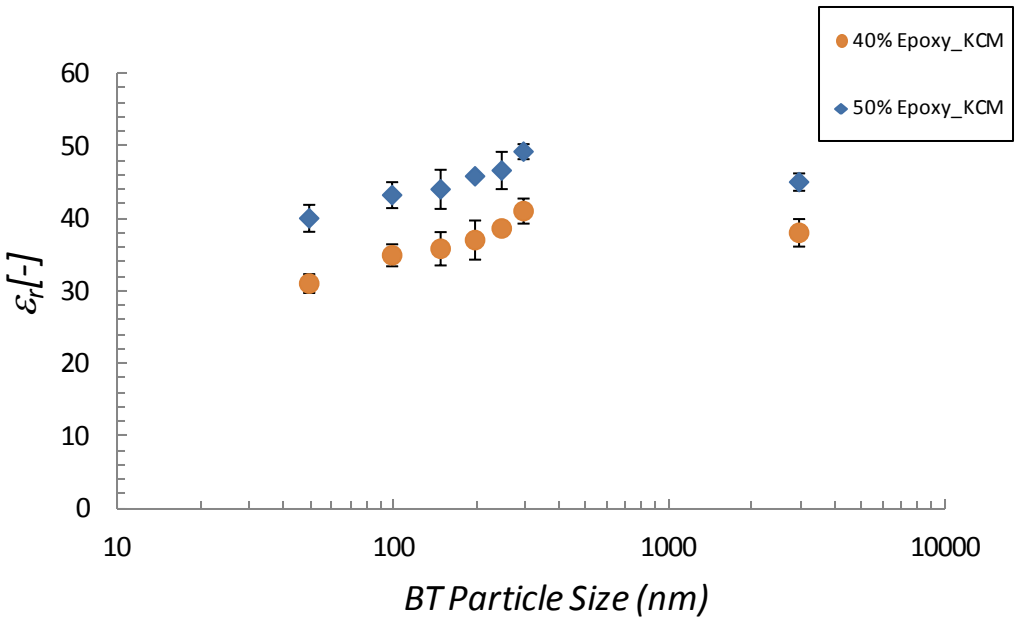

Figure 37: Dielectric properties of BT/Epoxy composites

4. 2. PZT/Epoxy Composite

The two phase PZT/Epoxy composites were fabricated by the following route. The PZT was mixed with Epoxy part A in a speedmixer for 5 mins at 2500 rpm. This was followed by mixing it with Epoxy part B in speedmixer for 5 mins at 2500 rpm. The resultant mixture was set for deairing procedure in a degassing chamber for 15 mins. After this, the mixture was again mixed in the speedmixer at 2500 rpm for 5 mins to get the uniform dispersion of the sedimented ceramic filler. This mixture was then poured into the Teflon mould and clamped tightly by the Al plates. The rest of the procedure involving dielectrophoresis, polishing & gold sputtering, and poling is kept same as mentioned in the previous chapter. This series of composites were fabricated by 5, 10, 15, and 20 vol% PZT. The dielectric and piezoelectric constants of this series of composites would be set as reference to evaluate the improvement in the piezoelectric properties by the addition of BT ceramic fillers to the PZT/Epoxy composite.

The piezoelectric properties of both random and structured composites are shown in fig. 38. The dielectric constant of both, random and structured, composites increases with the PZT volume fraction. The dielectric constant for the random composites is also compared with the Yamada model. To fit the Yamada model to the experimental data, the fitting parameter value was set to 7.3. The structured composites show higher dielectric constant the random composites for similar PZT volume fraction. The reason being the particle connectivity in a random composite is limited while the effective volume fraction of the ceramic filler is higher in the direction of the applied electric field for the structured composites. The piezoelectric charge constant increases with the PZT volume fraction, having a significantly higher value for the structured composites. This improvement in

properties (d33) for the structured composites is due to the 1-3 connectivity leading to quasi continuous ceramic path between the gold electrodes.

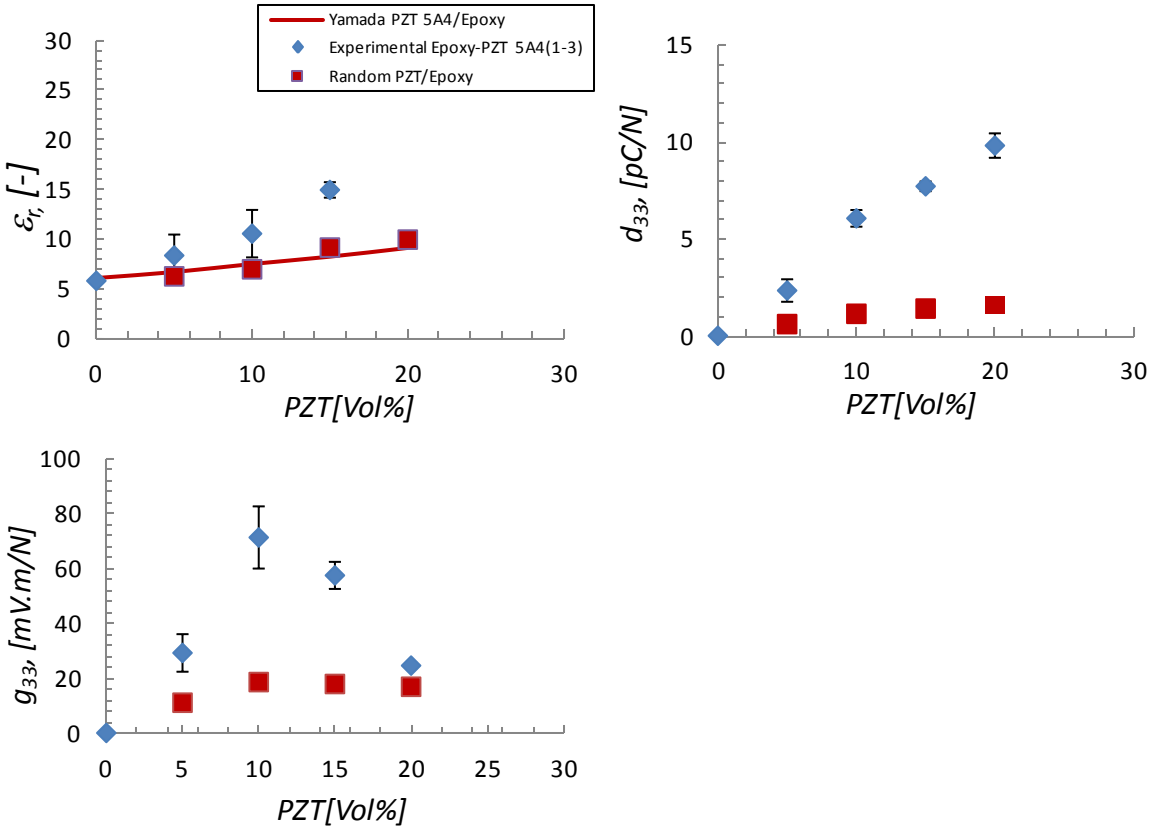

Figure 38: Piezoelectric properties of two phase PZT/Epoxy composites

The piezoelectric voltage constant increases with the PZT vol% until a certain threshold, for both random and structured composites. As expected, the g_{33} is higher for the structured composites than the random composites at similar PZT volume fraction. The g_{33} peaks at 10vol% PZT. After this PZT volume fraction, the g_{33} for structured composites reduces drastically. The obtained values are comparable to previous studies [14, 17]. The maximum g_{33} value of 70 mVm/N will be used as reference for the three phase composites that will be discussed in the following sections.

5. THREE PHASE COMPOSITES

This chapter will cover all the experimental studies pertaining to the three phase piezoelectric composites synthesised. The fabrication route and characterisation results will be discussed here. First the BT/PZT/epoxy composite is synthesised by using BT of particle size 3um. This is followed by synthesis of another series of BT/PZT/epoxy composites by using BT of particles size varying form 30-300 nm. Finally, the piezoelectric constants for both the series are then compared with that of PZT/epoxy composites to evaluate the improvements in the properties due to the addition of BT.

BT/PZT/Epoxy composites were made following a synthesis route almost similar to other composites discussed so far. PZT and Epoxy part A were mixed in a speedmixer at 2500 rpm for 5 mins, followed by addition of BT of particle size 3um to the mixture. This mixture is again mixed in the speedmixer to get a homogeneous ceramic filler distribution. Finally, Epoxy Part B is added to the mixture and again mixed in speedmixer at 2500 rpm for 5 mins. This is then set for deairing process in a degassing chamber for 15 mins. This is done to reduce the porosity in the final composites. These series of composites were synthesised with 2, 5 and 10 vol% of BT & 10 vol% of PZT. The rest of procedure involving dielectrophoresis, surface polishing, gold sputtering, and Poling conditions are kept same.

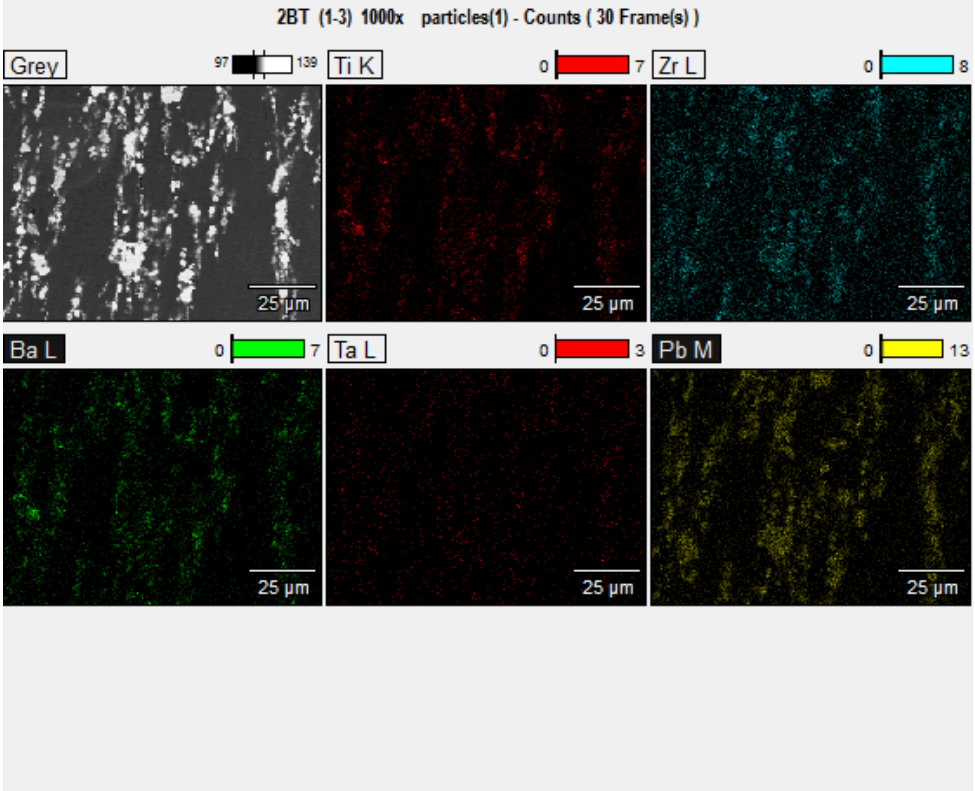

Figure 39: EDX results of structured BT/PZT/ Epoxy composites

Fig. 39 shows the SEM and EDX results for the structured three phase composites. The cross-sections of the synthesis three phase composites were first polished and gold sputtered before analysing them via SEM/EDX. The micrographs show how the two different ceramic fillers are orientated in one direction. The EDX results dearly show the vertical arrangement of both Lead (Pb) and Barium (Ba), implying chain like structuring of both BT and PZT particles. Some clustering of PZT particles was also observed. The EDX couldn't reveal much about the PZT and BT ceramic particle location with respect to each other. This is important to understand how the addition of BT ceramic filers affects the PZT particles vertical orientation. So, further line analysis was done as shown in fig. 40. It revealed that the BT particles in most cases are stacked in between PZT particles. The blue curve signifies the probable intensity (counts) of the presence of Barium, indicating BT particles at peaks. These results were similar for BT with different volume fraction.

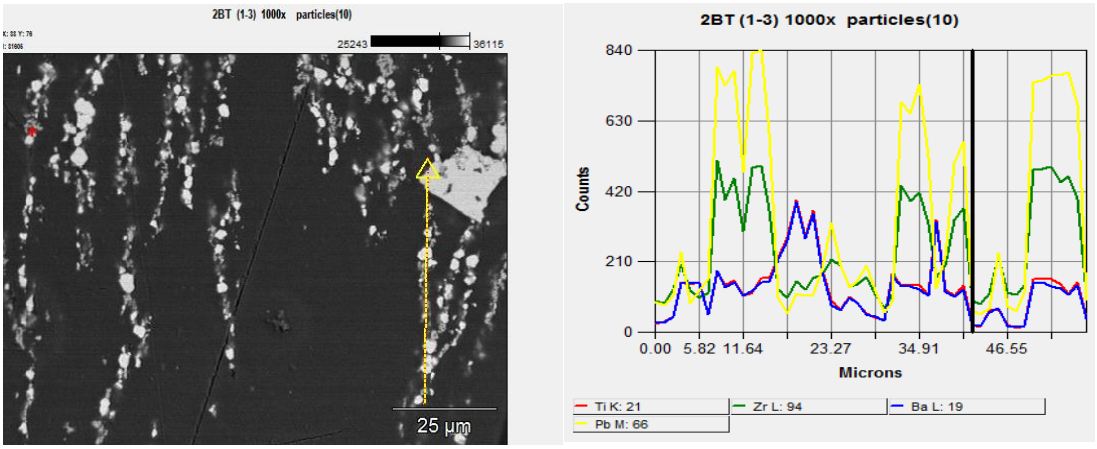

Figure 40: Line analysis for determining BT and PZT location precisely. Yellow peaks in the graph indicates PZT particle while the blue peaks indicates BT

The piezoelectric properties are depicted in fig. 41. The dielectric constant of random and structured composites increases with the BT volume fraction. This is expected since we are adding high dielectric constant ceramic filler to PZT/epoxy system. The piezoelectric charge constant also follows the similar trend indicating that the addition of BT has indeed led to better poling of the composites due to reduction in the dielectric mismatch. Though, this increase is not consistent as seen at BT 10 vol%. This indicates that there is a certain threshold at which further addition of BT ceramic particles doesn't influence the ceramic partide structuring and poling of the composites. The piezoelectric voltage constant for the structured composites on the other hand decreases with the BT volume fraction. This could be due to insignificant improvement in the poling efficiency of the composites. The piezoelectric voltage constant though increases for the random composites with the BT volume fraction. Hence this indicates that the poling efficiency for the random composites improved.

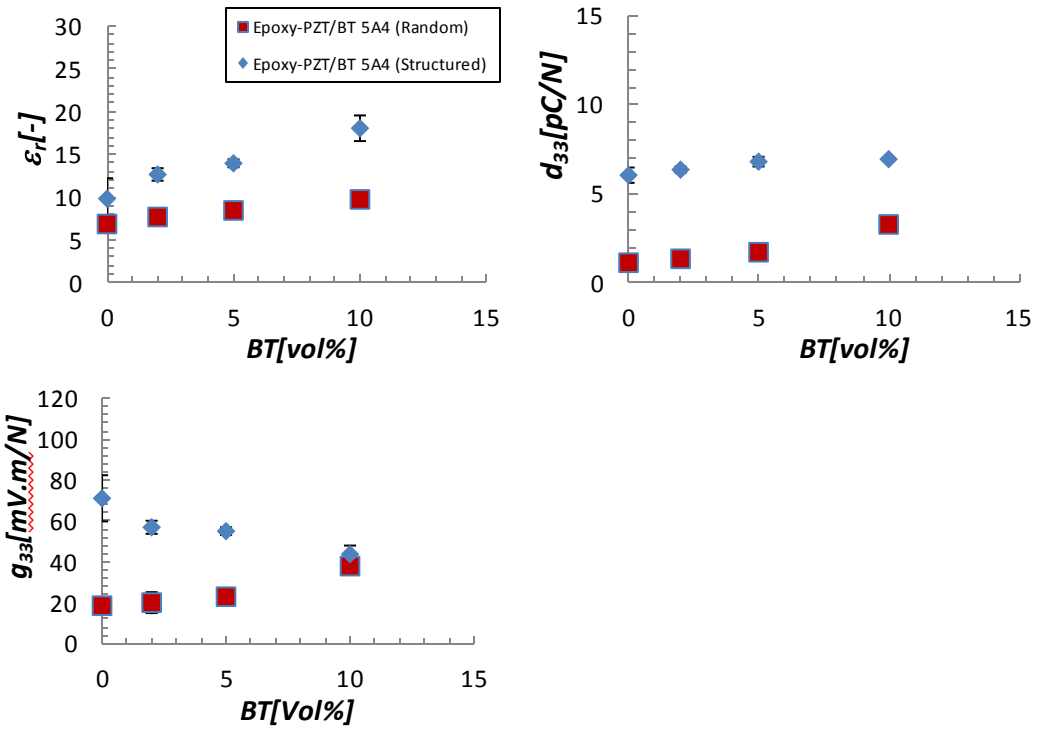

Figure 41: Piezoelectric properties of three phase BT/PZT/Epoxy composites with BT with a particle size of 3000 nm

5. 1. Nanoparticle Agglomeration

The 3 phase BT/PZT/Epoxy composites are hereafter made with the addition of BT nanopartides. PZT and Epoxy part A were first mixed in a speed-mixer at 2500 rpm for 5 mins, followed by addition of BT nanopartides to the mixture. This mixture is again mixed in the speed-mixer to get a homogeneous ceramic filler distribution. Finally Epoxy Part B is added to the mixture and again mixed in speedmixer at 2500 rpm for 5 mins. These series of composites were synthesised with 2, 5 and 10 vol% of BT & 10 vol% of PZT. The rest of procedure involving dielectrophoresis, surface polishing, gold sputtering, and Poling conditions are kept same. In this series BT of particle size 30, 50, 60, 100, and 150nm are used.

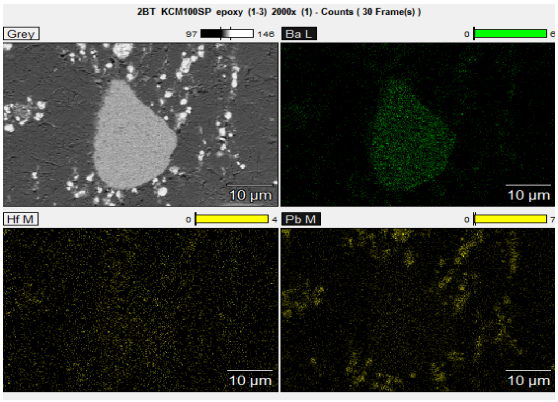

Figure 42: EDX results of Structured PZT/ BT/Epoxy Composite

The SEM and EDX results are shown in fig. 42 and fig. 43. Large grey clusters of BT nanoparticles surrounded by bright white PZT particles can be observed in the SEM images. The EDX results clearly shows clustering of Barium (Ba) surrounded by lead (Pb), implying agglomeration of BT nanoparticles. It can be easily concluded from these results that there is heavy agglomeration of BT nanoparticles due to the high surface energy of the nanoparticles. The particles structuring observed in the SEM results are similar to a Bi-modal particle arrangement, having a combination of small particles and large particle clusters and so there is indeed an improvement in the particle connectivity.

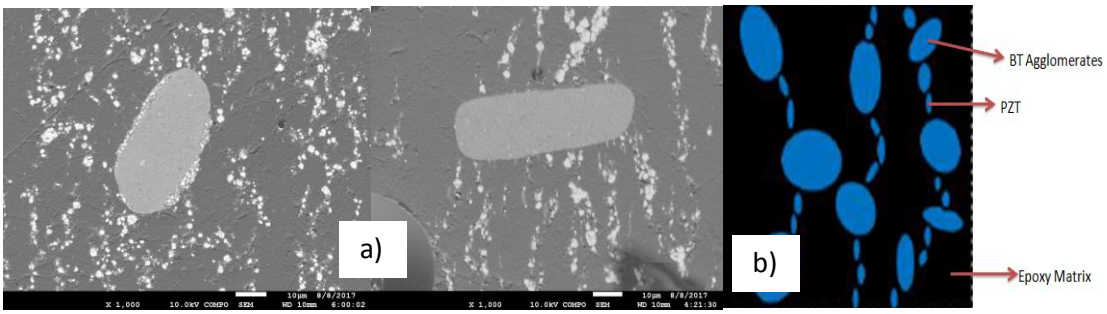

Figure 43: a) SEM micrographs of BT/PZT/Epoxy composite at 1000x magnification, b) Bi-modal Particle arrangement schematics [96]

The piezoelectric properties are shown in fig. 44 and fig. 45. The dielectric constant for both, random and structured, composites increases with the BT volume fraction. This is expected due to the addition of high dielectric constant BT nanopartides. Though, the variation in dielectric constant with different BT particles size is insignificant. This could be due to low volume fraction of BT nanoparticles used. The piezoelectric charge constant also increases with the BT volume fraction in spite of the presence of heavy BT agglomeration. This can be possibly explained by the fact that the resultant particles structuring in this series of composites was comparable to a Bi-Modal particles structuring, which can lead to improved particle connectivity. Again there is not much variation observed in the piezoelectric charge constant with the varying BT particle size. The BT particles size was observed to just influence the degree of agglomeration and the size of agglomerates, but the overall particle structuring remained same.

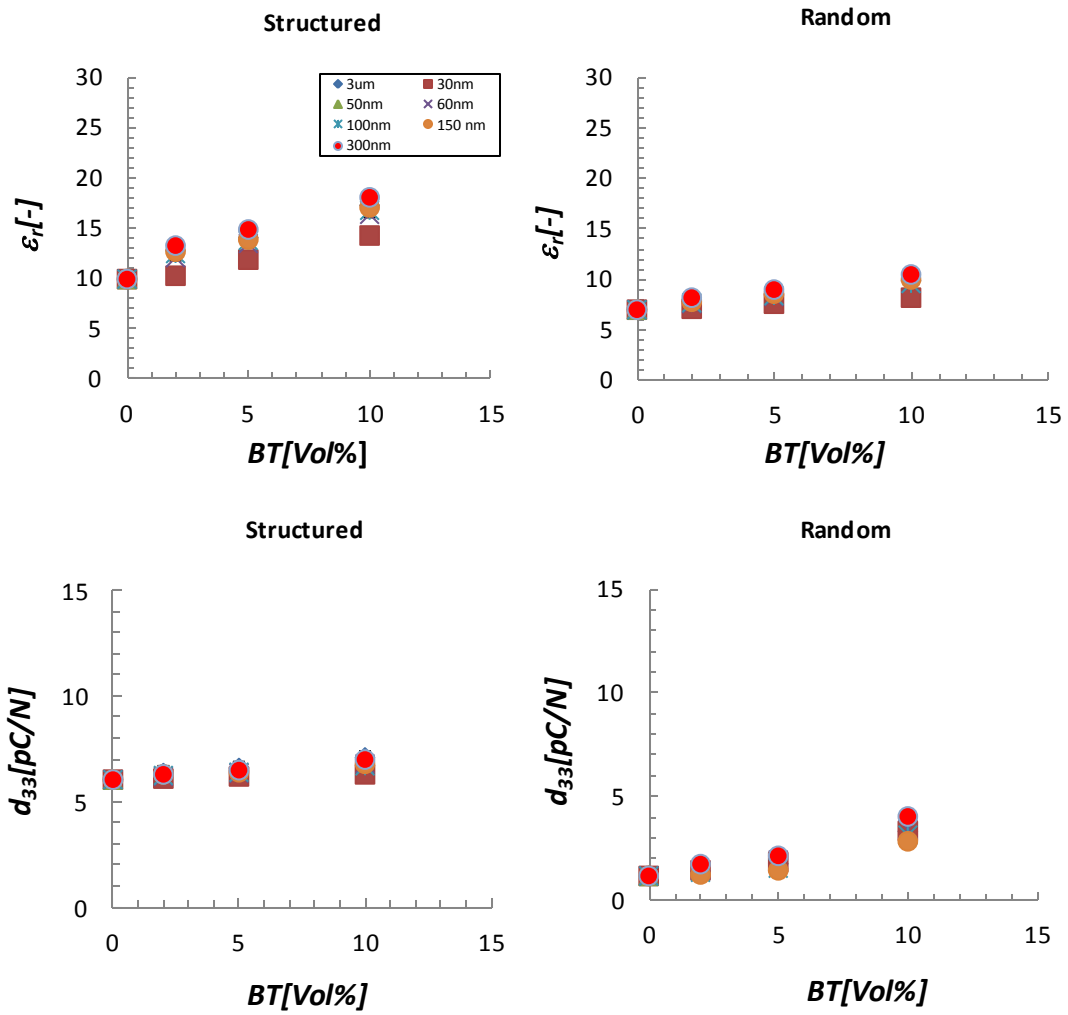

Figure 44: Dielectric and piezoelectric charge constant results of three phase BT/PZT/Epoxy composites with nanoparticles BT

The piezoelectric voltage constant for this series increases with the BT volume fraction for random composites and decreases with the BT volume fraction for structured composites. The addition of BT nanoparticles didn't lead to significant improvement in the poling efficiency of the composites due to the heavy BT agglomeration. Hence there is no significant improvement in the g_{33} properties of this series with the addition of BT nanoparticles.

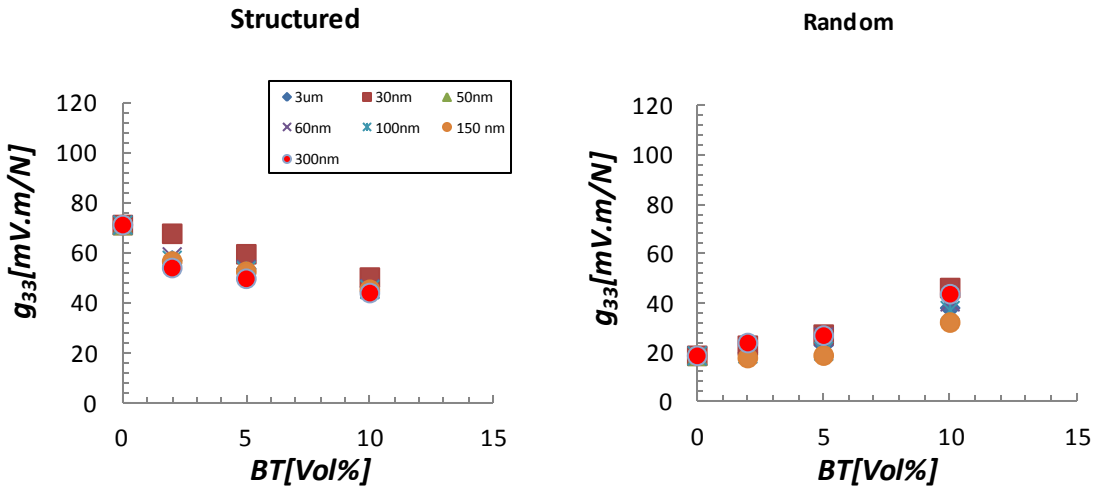

Figure 45: Piezoelectric properties of BT/PZT/Epoxy composites

5. 2. Ultrasonication

As we have seen in the previous section the addition of BT nanoparticles did lead to heavy agglomeration of the nanoparticles in the final composites. In an attempt to reduce the degree of agglomeration a modification was made into the synthesis route of the 3 phase BT/PZT /Epoxy composites. The BT nanoparticles and Epoxy part B are first mixed in a speed mixer at 2500 rpm for 5 mins. Epoxy part B is used for this step due to its low viscosity and hence being more effective in the ultrasonication procedure. This mixture is then placed in an ultrasonic bath, via the method which is called indirect ultrasonication, for 1 hr in an ultrasonic bath filled with ethanol (fig. 46). After the ultrasonication procedure, the PZT powder is added to the mixture and mixed in a speedmixer at 2500 rpm for 5 mins. Finally, Epoxy part A is the added and mixed again in the speedmixer for 5 mins at 2500 rpm. The rest of the fabrication route including dielectrophoresis, gold sputtering and poling conditions are kept same.

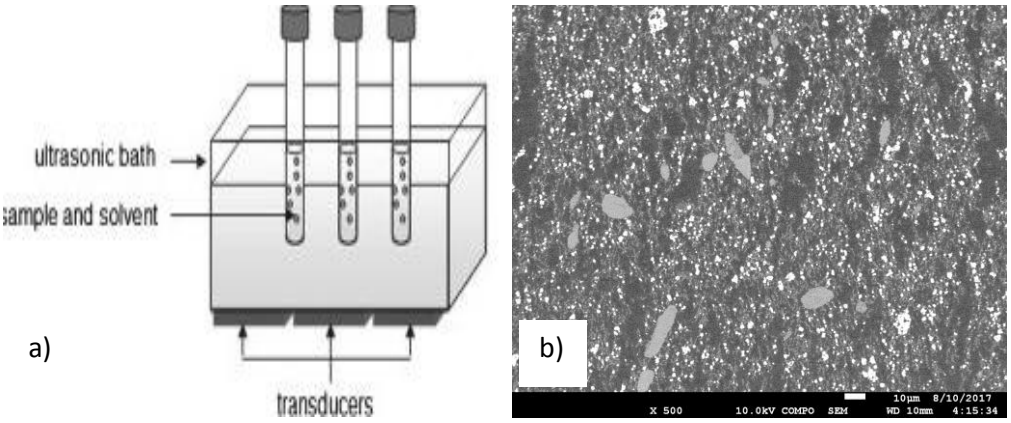

Figure 46: a) Indirect Ultrasonication Setup b) SEM micrograph of Ultrasonicated PZT/BT/epoxy composite

The SEM image above clearly shows significant reduction in the size of BT nanoparticle agglomerates. Though the agglomerates are not completely broken and their distribution remains same. This can be explained by the fact that the deagglomerated nanoparticles after the ultrasonication procedure have the tendency to agglomerate again with time.

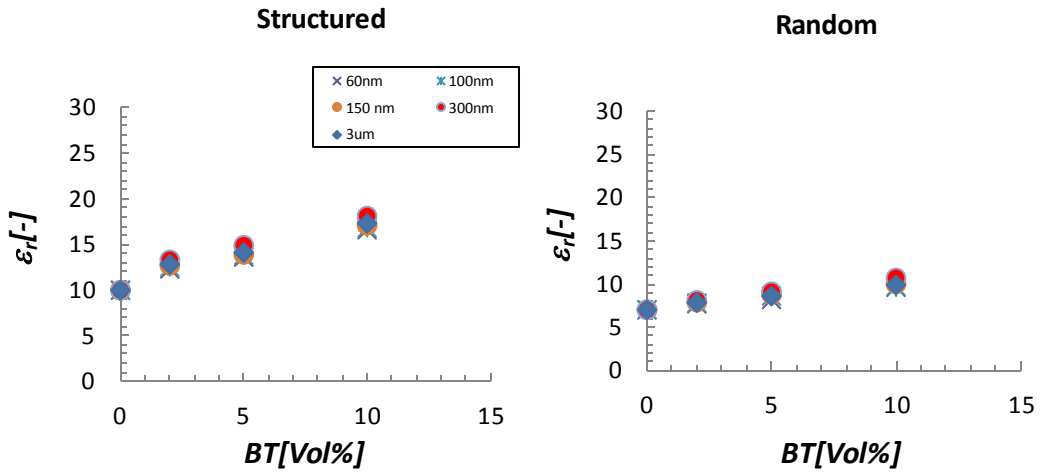

Figure 47: Dielectric properties of BT/PZT/Epoxy composites made from Ultrasonication route

The piezoelectric properties are shown in figure. The dielectric constant for both, random and structured, composites increases with the BT volume fraction. This is expected, as we have seen in the previous composite series, due to the addition of high dielectric constant BT nanoparticles. The effect of ultrasonication on the dielectric constant is insignificant since the particle structuring remains same while there is only reduction in the size of agglomerates. The variation in dielectric constant with different BT particles size is again insignificant due to the low volume fraction of BT nanoparticles used. The piezoelectric charge constant also increases with the BT volume. The decrease in the size of BT nanopartide agglomerates leads to improved bi-modal particles arrangement causing improved particles connectivity.

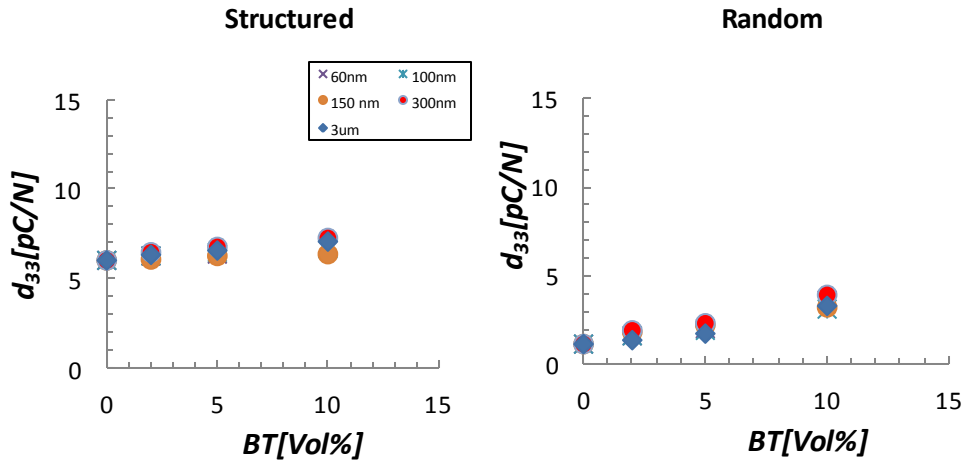

Figure 48: Piezoelectric properties of Ultrasonicated BT/PZT/epoxy composites

The piezoelectric voltage constant for this series increases with the BT volume fraction for random composites and decreases with the BT volume fraction for structured composites. The addition of BT

nanoparticles didn't lead to significant improvement in the poling efficiency of the composites due to the presence of BT agglomerates and absence of BT nanopartides between micro sized PZT particles. Effectively, there is no reduction in the dielectric mismatch between the ceramic filler and the polymer matrix that was expected with the addition of BT nanoparticles. Hence there is no significant improvement in the g_{33} properties of this series with the addition of BT nanoparticles.

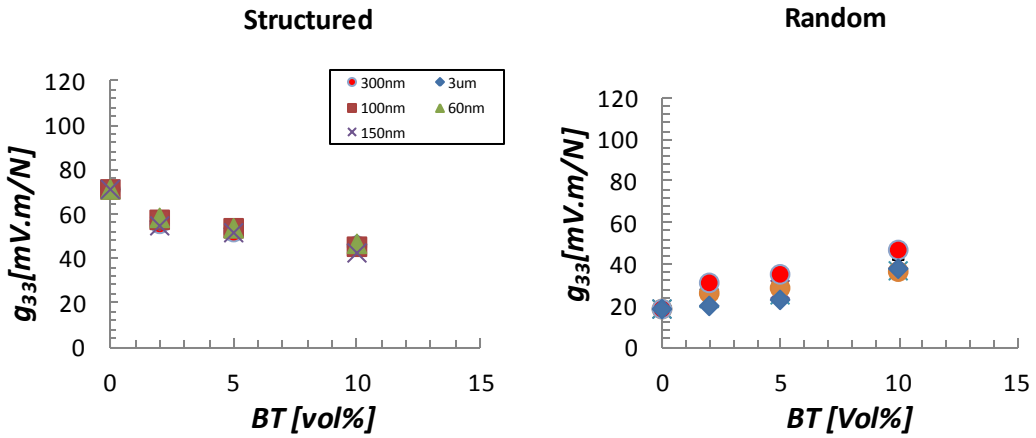

Figure 49: Piezoelectric properties of Ultrasonicated BT/PZT/epoxy composites

5. 3. Powder Mix

In an attempt to improve the ceramic particle structuring and reducing BT nanoparticles agglomeration in the 3 phase BT/PZT/Epoxy composites, a different synthesis route was used. The two ceramic fillers were mixed together instead of using them separately as done in the 3 phase composites made earlier. The main motivation behind adopting this particular route was to get a homogeneous dry mixture of ceramic fillers which could potentially improve the particle distribution and structuring in the polymer matrix. PZT and BT nanoparticles were mixed in a speed mixer at 3500 rpm for 5 mins to get a homogeneous ceramic powder mixture. The epoxy part-A and part-B were then added to this powder mix and mixed again in speed mixer at 2500 rpm for 5 mins. This mixture was then deaired in a degassing chamber for 15 mins. This mixture was then poured in Teflon moulds and was allowed to cure at 100°C for 3 hrs. The rest of the fabrication procedure involving dielectrophoresis, gold sputtering and poling is kept same.

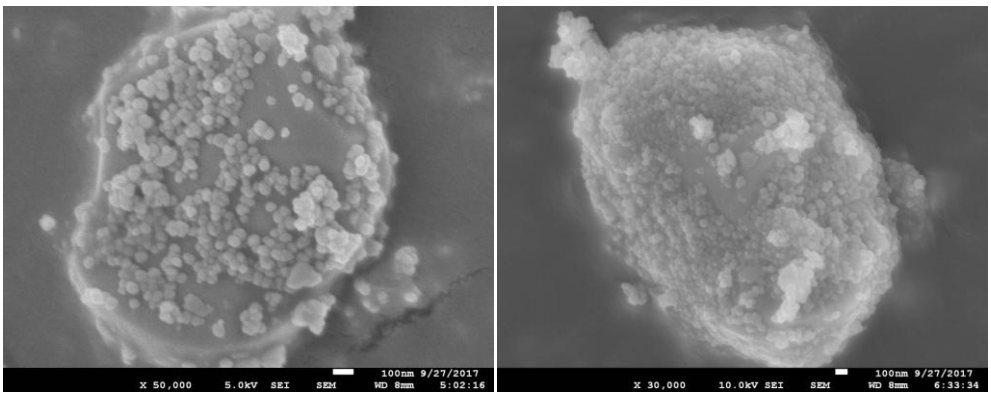

Figure 50: SEM micrographs of dry powder mix of PZT and BT

The SEM micrograph of the dry powder mix is shown above. These micrographs clearly show the coating of BT nanoparticles over the micron sized PZT particles. The clustering of BT nanoparticles over the PZT surface was best observed for 30nm and 60nm partide sizes. The EDX results show vertical stacking of both Barium (violet) and (red). Also comparing this with the SEM micrograph it can be seen that the BT nanoparticles are indeed clustered around the micron sized PZT partides. This is in contrast to the particle structuring of previous composites where only the PZT particles are seen to be vertically aligned. The SEM micrograph clearly shows chain like structuring of both PZT and BT particles, where the large white partide are PZT micron sized particles and the violet colour particles depicts BT nanoparticles.

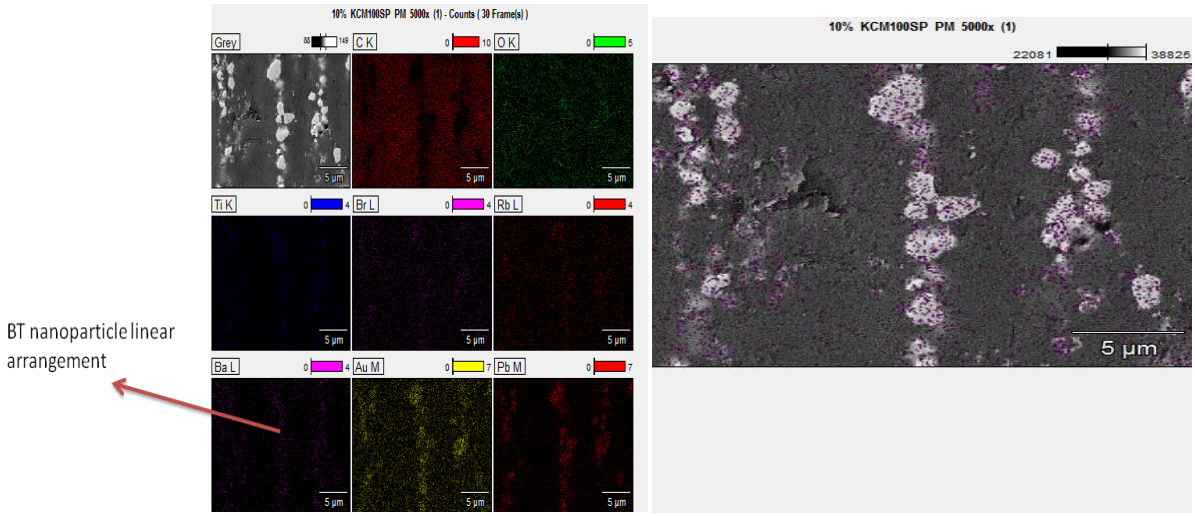

Figure 51: EDX results of powder mixed PZT/BT/Epoxy composites.

The piezoelectric properties are shown in fig. 52 and fig. 53. As expected there is significant improvement in the dielectric constant and piezoelectric charge constant values for the 3 phase BT/PZT/epoxy composites. The trends are similar to the results from the previously made composites. For both random and structured composites the dielectric constant increases with the increase in BT volume fraction. The variation in the dielectric constant due to partide size was not significant, possibly due to low BT volume fraction. The piezoelectric charge constant for both random and structured composites increases with the BT volume fraction. Here we can also notice that the properties of composites with 60nm and 300nm BT dominates.

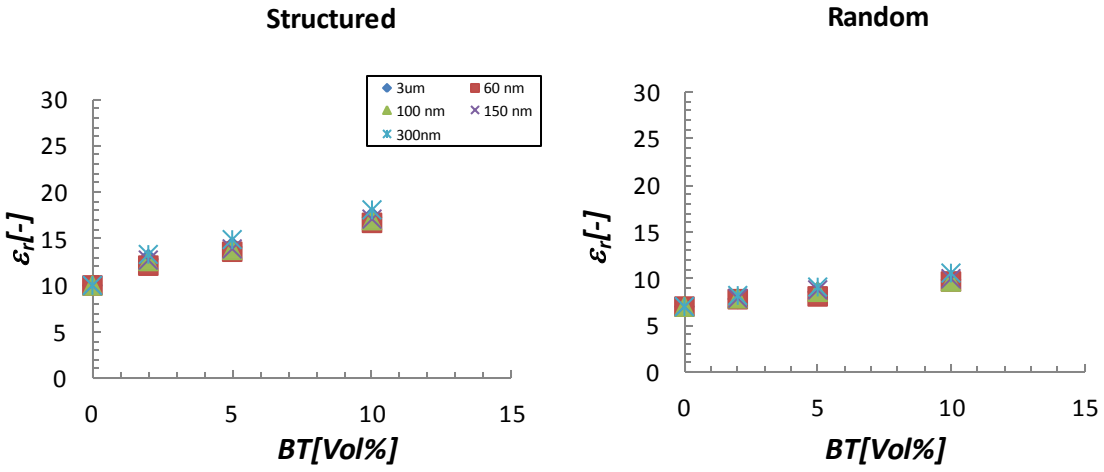

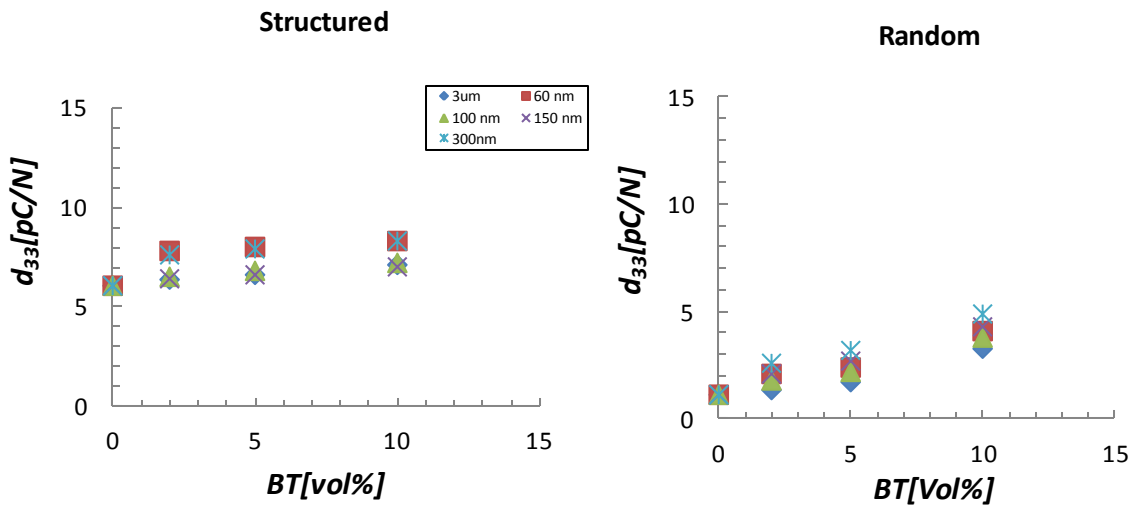

Figure 52: Dielectric and piezoelectric properties of BT/PZT/Epoxy composites

As for the piezoelectric voltage constant, the trend for both random and structured composites is almost similar to the previously made composites. The structured composites showed a maximum value of 80mVm/N at 2 vol% BT. After this point the voltage constant decrease drastically with the increase in BT volume fraction. The composites with BT particle size 60nm give significantly higher voltage constants in comparison with other BT particles sizes. This could be possibly due to the lowest possible dielectric mismatch between the 60nm BT particles and PZT particles. This leads to better polling efficiency and hence higher piezoelectric properties.

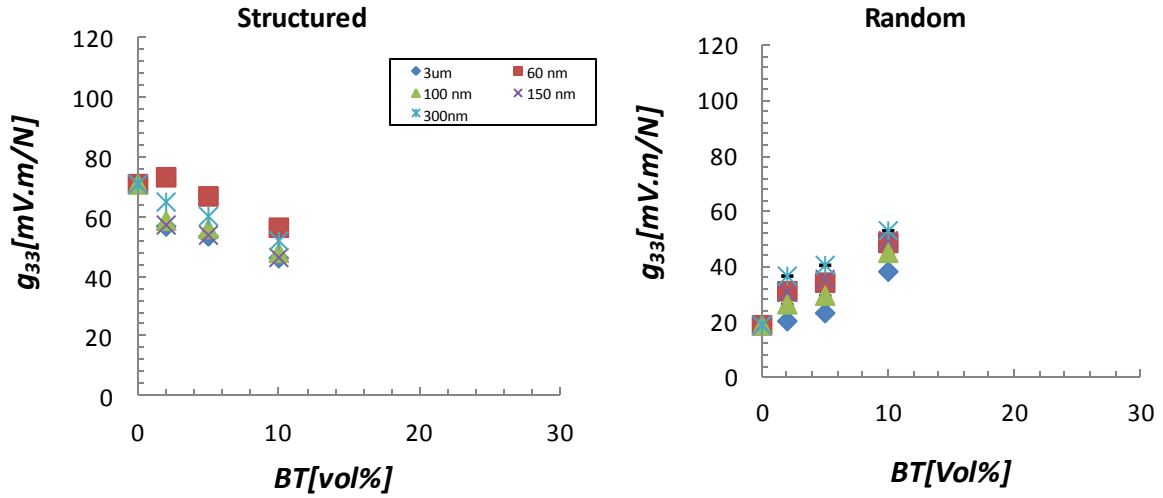

Figure 53: Piezoelectric properties of the PZT/BT/Epoxy composites made by powder mix route

It can be seen that even though there was an improvement in the piezoelectric properties of the composite with the addition of BT nanoparticles, the improvements were not high enough to justify the use of BT nanoparticles and adopt a complex synthesis route. The main reason behind this could be due to the improper dispersion of the BT nanoparticles in the epoxy matrix. The BT nanoparticles were mostly clustered around the micron sized PZT particles rather than being in between two PZT particles, as shown in the fig. 54. Hence the end result was still a significant dielectric mismatch affecting the polling efficiency.

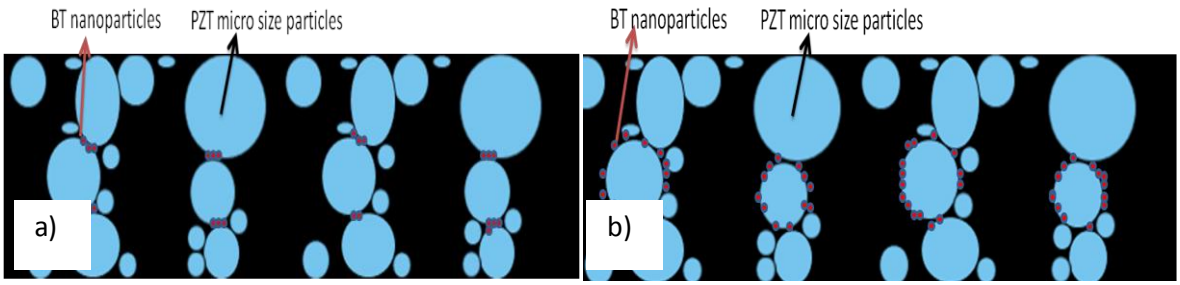

Figure 54: a) Schematics showing Ideal nanoparticle structuring b) observed Nanoparticles Structuring

6. CONCLUSIONS

The main objective of this thesis project was to evaluate if the three phase composite system fabricated by addition of BT nanoparticles leads to a significant improvement in the piezoelectric properties. So it was majorly a proof of concept study where the aim was to improve the ceramic particles connectivity in a polymer matrix by the inclusion of different ceramic filler (nanoparticles) in a quasi 1-3 composite. If enhanced particle structuring is achieved, there would be a drastic reduction in the dielectric mismatch leading to enhanced poling efficiency and hence better piezoelectric properties. The methodology involved reproducing results for PZT/Epoxy composites for reference, followed by fabrication of three phase composites by addition of BT ceramic filler of 3 μm. Finally BT nanoparticles were added to evaluate the improvement in the properties.

It was concluded that the piezoelectric properties did improve with the addition of high dielectric constant BT nanoparticles, but the improvements were lower than expected. The EDX and SEM results contributed in the understanding the reason behind the observed piezoelectric properties. It was observed that the particle structuring of BT nanoparticle and PZT particles were far from ideal. The BT nanoparticles were clustered around the micron sized PZT particles instead of being concentrated in between subsequent PZT particles. Hence the dispersion of BT nanoparticles in the Epoxy polymer matrix was the problem.

In an attempt to improve the particle dispersion, Ultrasonication and powder mix techniques were used. The powder mix fabrication route proved to be more effective than the ultrasonication procedure. It was observed that the BT nanoparticles were clustered over the surface of PZT particles, which significantly helped in dispersion of the nanoparticles around the PZT particles. Also the composite with 2vol% BT showed the highest piezoelectric charge constant in structured composites.

The effect of BT particle size on the piezoelectric properties of the composites was concluded to be insignificant though this can change if the perfect dispersion of the BT nanoparticles is achieved. Also it was proved that the dielectric constant of the BT ceramic filer is dependent on its particle size in the nanoscale region. The maximum dielectric constant was found to be at 300nm irrespective of the polymer matrix and BT volume fraction.

For this project a number of recommendations can be given for any future research. Before conducting the experimental studies, a more in-depth theoretical analysis of nanoparticle agglomeration and their dispersion in the polymer matrix needs to be established. Use of nanoparticle surfactants should be explored, but keeping in consideration that the surfactants itself didn't influence the electrical properties of the composites. Optimization studies needs to be conducted to get the required particles structuring.

Also the effect of dielectrophoresis on the nanoparticle alignment in the polymer matrix needs to be further explored. The AC voltage and frequency could be optimised to achieve the required particles connectivity. Also poling efficiency needs to be determined by measuring the hysteresis loops.

BIBLIOGRAPHY

1. M. Wahbah, M. Alhawari, B. Mohammad, H. Saleh and M. Ismail, *Characterization of Human Body-Based Thermal and Vibration Energy Harvesting for Wearable Devices*, IEEE Journal **4**, 354 (2014).

2. P. Hiralal, H.E. Unalan and G.A.J. Amaratunga, *Nanowires for Energy Generation*, Nanotechnology **23**, 194002 (2012).

3. H. Li, C. Tian and Z.D. Deng, *Energy Harvesting from Low Frequency Applications Using Piezoelectric Materials*, Applied Physics Reviews **1**, 041301 (2014).

4. C. Wong, Z. Dahari, A.A. Manaf and M.A. Miskam, *Harvesting Raindrop Energy with Piezoelectrics*, Journal of Electronic Materials **44**, 13 (2015).

5. H. Abdi, N. Mohajer and S. Nahavandi, *Human Passive Motions and a User-friendly Energy Harvesting System*, Journal of Intelligent Material Systems and Structures **25**, 923 (2014).

6. J. Holterman and P. Groen, *An Introduction to Piezoelectric Materials and Applications*, 1st ed., Stichting Applied Piezo, Apeldoorn (2013).

7. W. D. Callister, *Materials Science and Engineering: An Introduction*, 7th ed., John Wiley & Sons (2007).

8. B. Jaffe, W. R. Cook, and H. Jaffe, *Piezoelectric ceramics*, Academic Press, London, New York (1971).

9. G. H. Haertling, *Ferroelectric ceramics: history and technology*, Journal of the American Ceramic Society **82**, pp. 797-818 (1999).

10. A. Safari, *Development of piezoelectric composites for transducers*, Journal de Physique III **4**, pp. 1129-1149 (1994).

11. R.E. Newnham, *Composite Electroceramics* , Ferroelectrics **68**, 1(1986).

12. R.E. Newnham, A. Safari, J. Giniewicz, and B.M. Fox, *Piezoelectric Sensors,* Ferroelectrics **60**, 15 (1984).

13. R. Dittmer, W. Jo, K. G. Webber, J. L. Jones, and J. Rödel, *Local structure change evidenced by temperature-dependent elastic measurements: Case study on $Bi_{1/2}Na_{1/2}TiO_3$-based lead-free relaxor piezoceramics*, Journal of Applied Physics **115**, p. 084108 (2014).

14. K.H. Lam, X. Wang, and H.L.W. Chan, *Piezoelectric and pyroelectric properties of $(Bi_{0.5}Na_{0.5})_{0.94}Ba_{0.06}TiO_3$/P(VDF-TrFE) 0–3 composites*, Composites Part A: Applied Science and Manufacturing **36**, pp. 1595-1599 (2005).

15. D. Van den Ende, B. Bory, W. Groen, and S. Van der Zwaag, *Improving the d_{33} and g_{33} properties of 0-3 piezoelectric composites by dielectrophoresis*, Journal of Applied Physics **107**, p. 024107 (2010).

16. D. Van den Ende, *Structured Piezoelectric Composites- Materials and Applications*, PhD Dissertation, Novel Aerospace Materials, TU Delft (2012).

17. N. K. James, *Piezoelectric and dielectric properties of polymer-ceramic composites for sensors*, PhD Dissertation, Novel Aerospace Materials (NOVAM) Delft University of Technology, Delft Netherlands (2015).

18. G. S. Gong, A. Safari, S. Jang, and R. Newnham, *Poling flexible piezoelectric composites*, Ferroelectrics Letters Section **5**, pp. 131-142 (1986).

19. K. Lam, M. Guo, D. Lin, K. Kwok, and H. Chan, *Lead-free piezoelectric BNKLT 1–3 composites*, Journal of Materials Science **43**, pp. 1677-1680 (2008).

20. N.A. Masacrenhas, *Flexible & Structured Piezoelectric Composites for Vibration Damping*, MSc. Thesis, TU Delft (2015).

21. R. Popielarz, *Dielectric Properties of Polymer/Ferroelectric Ceramic Composites from 100 Hz To 10 Ghz*, Macromolecules **34**, pp. 5910-5915 (2001).

22. J. Obrzut and R. Nozaki, *Proceedings of the IPC EXPO Technical Conference*, San Diego, CA April 2-8 (2000).

23. V.S. Dalle, *The Effect Of Processing Conditions On The Morphology, Thermomechanical, Dielectric, And Piezoelectric Properties Of P(VDF-Trfe)/Batio3 Composites*, Journal of Materials Science **47**, pp. 4763-4774 (2012).

24. H.L.W. Chan, M.C. Cheung and C.L. Choy, Ferroelectrics **224**, pp. 541-545 (1999).

25. Y.P. Mao, S.Y. Mao, Z.G. Ye, Z.X. Xie, L.S. Zheng, *Size-dependences of the dielectric and ferroelectric properties of $BaTiO_3$ polyvinylidene fluoride nanocomposites*, Journal Applied Physics **108**, 014102 (2010).

26. T. R. Gurutaja, *Piezoelectric transducers for medical ultrasonic imaging*, American Ceramic Society Bulletin **73**, 50 (1994).

27. V. F. Janas and A. Safari, Journal American Ceramic Society **78**, 2949 (1995).

28. L.F. Chen, *Preparation and Properties of Polymer Matrix Piezoelectric Composites Containing Aligned $BaTio_3$ Whiskers*, Journal of Materials Science **39**, pp.2997-3001 (2004).

29. L. F. Chen and C. Leonelli, *Alignment if Silicon-Carbide Whiskers in Polymer Matrix*, Journal Material Science **32**, pp. 627-631 (1997).

30. D. M. Bigg, Polymer Engineering Science **19**, pp. 1188 (1997).

31. K. T. Chung, A. Sabo and A. P. Pica*, Electrical permittivity and conductivity of carbon black-polyvinyl chloride composites*, Journal Applied Physics **53**, pp. 6867 (1982).

32. Lin, Yirong, and Henry A. Sodano, *Fabrication and Electromechanical Characterization of a Piezoelectric Structural Fiber for Multifunctional Composites*, Advanced Functional Materials **19**, pp. 592-598 (2009).

33. J. W. Kim and J. G. Heinrich, *Influence of Processing Parameters on Microstructure and Ferroelectric Properties of PZT-Coated SiC Fibers*, Journal European Ceramic Society **25**, 1637 (2005).

34. Bowland, Christopher, Zhi Zhou, and Henry A. Sodano, *Multifunctional Barium Titanate Coated Carbon Fibers*, Advanced Functional Materials **24**, pp. 6303-6308 (2014).

35. Choi and Woongchul*, Improving Piezoelectric Performance of Lead-Free Polymer Composites with High Aspect Ratio $BaTio_3$ Nanowires*, Polymer Testing **53**, pp. 143-148 (2016).

36. Y. Yang, W. Guo, K.C. Pradel, G. Zhu, Y. Zhou, Y. Zhang, Y. Hu, L. Lin, Z.L. Wang, *Pyroelectric Nanogenerators for Harvesting Thermoelectric Energy*, Nano Letters **12**, pp. 2833−2838 (2012).

37. Y. Saito, H. Takao, T. Tani, T. Nonoyama, K. Takatori, T. Homma, T. Nagaya, M. Nakamura, Lead-Free Piezoceramics, Nature **432**, pp. 84–87 (2004).

38. N. D. Spencer and J. H. Moore, *Encyclopedia of Chemical Physics and Physical Chemistry* ,Institute of Physics Publishing, Bristol, UK (2001).

39. C.P. Bowen, T.R. Shrout, R.E. Newnham, A study of the frequency dependence of the dielectrophoretic effect in thermoset polymers, Journal of Materials Research **12**, pp. 2345–2356 (1997).

40. C. Park and R.E. Robertson, *Aligned microstructure of some particulate polymer composites obtained with an electric field*, Journal Material Science **33**, pp. 3541 (1998).

41. Lin and Zong-Hong, *$BaTio_3$ nanotubes-Based Flexible and Transparent Nanogenerators*, The Journal of Physical Chemistry Letters **3**, pp. 3599-3604 (2012).

42. D.V. Bavykin, V.N. Parmon, A.A. Lapkina, F.C. Walsh*, The Effect of Hydrothermal Conditions on the Mesoporous Structure of TiO_2 Nanotubes*, Journal Material Chemistry **14**, pp. 3370−3377 (2004).

43. Y. Wei, Y. Song, X. Deng, B. Han, X. Zhang, Y. Shen, Y. Lin, *Dielectric and Ferroelectric Properties of $BaTiO_3$ Nanofibers Prepared via Electrospinning*, Journal Material Science Technology **30,** pp. 743–747 (2014).

44. Y. M. Poon, C. H. Ho, Y. W. Wong, and F. G. Shin, Theoretical predictions on the effective piezoelectric coefficients of 0–3 PZT / polymer composites, Journal Material Science **42**, pp. 6011-6017 (2007).

45. K. Arlt and M. Wegener, *Piezoelectric PZT / PVDF-copolymer 0-3 composites: aspects on film preparation and electrical poling, Dielectrics and Electrical Insulation*, IEEE Transactions **17**, pp. 1178-1184 (2010).

46. B.S. Prakash and K. B. R. Varma, *Synthesis, characterization and gas sensing performance of SnO 2 thin films prepared by spray pyrolysis*, Composites Science Technology **67**, pp. 2363-2368 (2007).

47. Udhay Sundar, Dielectric And Piezoelectric Properties Of Percolative Three-Phase Piezoelectric Polymer Composites, Journal of Vacuum Science & Technology B, Nanotechnology and Microelectronics: Materials, Processing, Measurement, and Phenomena **34**, pp. 1232-1236 (2016).

48. H.W. Choi, Y.W. Heo, J.H. Lee, J.J. Kim, H.Y. Lee, E.T. Park, and Y.K. Chung, *Effects of $BaTiO_3$ on dielectric behavior of $BaTiO_3$-Ni-polymethyl methacrylate composites*, Applied Physics Letters **89**, pp. 132910-3 (2006).

49. Z. M. Dang, Y. Shen, and C. W. Nan, *Dielectric behavior of three-phase percolative Ni-$BaTiO_3$/polyvinylidene fluoride composites*, Applied Physics Letters **81**, pp. 4814-4816 (2002).

50. S. G. Miller and T. U. O. Akron, *Effects of Nanoparticle and Matrix Interface on Nanocomposite Properties*, The University of Akron (2008).

51. K.L. Park, Flexible *nanocomposite generator made of $BaTiO_3$ nanoparticles and graphitic carbons*, Advance Materials **24**, pp. 2999–3004 (2012).

52. M. Ma and X. Wang, *Preparation, microstructure and properties of epoxy-based composites containing carbon nanotubes and PMN-PZT piezoceramics as rigid piezo-damping materials*, Materials Chemistry and Physics **116**, pp. 191-197 (2009).

53. D. Carponcin, *Electrical and Piezoelectric Behavior of Polyamide/PZT/CNT Multifunctional Nanocomposites*, Advanced Engineering Materials **16**, pp. 1018-1020 (2014).

54. Z.M. Dang, *Tailored dielectric properties based on microstructure change in $BaTiO_3$-carbon nanotube/ polyvinylidene fluoride three-phase nanocomposites*, Journal Physical Chemistry C **114**, pp. 13204–13209 (2010).

55. S.H. Yao, *$BaTiO_3$ carbon nanotube/ polyvinylidene fluoride three-phase composites with high dielectric constant and low dielectric loss*, Applied Physics Letter **93**, pp. 182905 (2008).

56. S. Banerjee, *Piezoelectric And Dielectric Characterization Of Corona And Contact Poled PZT Epoxy-MWCNT Bulk Composites*, Smart Materials and Structures **25** pp. 115018-115029 (2016).

57. E.M. McKenna, *Comparison of r_{33} values for AJ404 films prepared with parallel plate and corona poling,* Journal of the Optical Society of America B **24**, pp. 2888–2892 (2007).

58. S. Huang, *Efficient poling of electro-optic polymers in thin films and silicon slot waveguides by detachable pyroelectric crystals*, Advance Materials **24,** pp. 42–47 (2012).

59. M. Hori, T. Aoki, Y. Ohira, and S. Yano, *New type of mechanical damping composites composed of piezoelectric ceramics, carbon black and epoxy resin*, Composites Part A: Applied Science and Manufacturing **32**, pp. 287-290 (2001).

60. J. Mao, *Piezoelectric and Dielectric Behavior of 0-3 Asphalt-Based Composites With Carbon Black*, Ceramics International **42**, pp. 16132-16137 (2016).

61. H. Kim, A.A. Abdala, and C.W. Macosko, Graphene/polymer nanocomposites Macromolecules **43**, pp. 6515–6530 (2010).

62. A. Javadi, *Chemically modified graphene/P(VDF-TrFE-CFE) Electroactive polymer nanocomposites with superior electromechanical performance*, Journal Materials Chemistry **22**, pp. 830–834 (2012).

63. N. Saber, *Superior Piezoelectric Composite Films: Taking Advantage Of Carbon Nanomaterials*, Nanotechnology **25** (2014).

64. L. Zaman, *Epoxy/graphene platelets nanocomposites with two levels of interface strength,* Polymer **52**, pp. 1603–1611 (2011).

65. M. Taneef, H. Saleem, and A. Habib, *Use Of Graphene Nanosheets And Barium Titanate As Fillers In PMMA For Dielectric Applications*, Synthetic Metals **223,** pp. 101-106 (2017).

66. Y. Li, *Graphene sheets segregated by barium titanate for polyvinylidene fluoride composites with high dielectric constant and ultralow loss tangent*, Composites Part A: Applied Science Manufacturing **78**, pp. 318–326 (2015).

67. H. W. Choi, Y. W. Heo, J. H. Lee, J. J. Kim, H. Y. Lee, E. T. Park, and Y. K. Chung, Integrated Ferroelectrics **87**, p. 85 (2007).

68. S. Banerjee and K. A. Cook-Chennault, Influence *of Al particle size and lead zirconate titanate (PZT) volume fraction on the dielectric properties of PZT-epoxy-aluminum composites*, Journal Engineering Materials Technology **133**, pp. 1-6 (2011).

69. S. Banerjee and K. A. Cook-Chennault, Composites Part A **43**, p. 1612 (2012).

70. S. Banerjee, W. Du, L. Wang, and K. A. Cook-Chennault, Journal of Electroceramics **31**, p. 148 (2013).

71. S. Banerjee, and K. A. Cook-Chennault, *Influence Of Aluminium Inclusions On Dielectric Properties Of Three-Phase PZT–Cement–Aluminium Composites*, Advances in Cement Research **26**, pp. 63-76 (2014).

72. J. M. Hwu, W. H. Yu, W. C. Yang, Y. W. Chen, and Y. Y. Chou, *Characterization of Dielectric Barium Titanate Powders Prepared by Homogeneous Precipitation Chemical Reaction for Embedded Capacitor Applications*, Materials Research Bulletin **40**, pp. 1662–1679 (2005).

73. P. K. Panda, *Review: environmental friendly lead-free piezoelectric materials*, Journal Materials Science **44**, pp. 5049–5062 (2009).

74. A. Gruverman and A. Kholkin, *Nanoscale ferroelectrics: processing, characterization and future trends*, Reports on Progress in Physics **69**, pp. 2443–2474 (2006).

75. J. Varghese, R.W. Whatmore and J.D. Holmes, *Ferroelectric nanoparticles, wires and tubes: synthesis, characterisation and applications*, Journal of Materials Chemistry C **1**, pp. 2618–2638 (2013).

76. T. Hoshina, H. Kakemoto, T. Tsurumi, S. Wada and M. Yashima, *Size and temperature induced phase transition behaviors of barium titanate nanoparticles*, Journal of Applied Physics **99** (2006).

77. W. Sun, *Size effect in barium titanate powders synthesized by different hydrothermal methods*, Journal of Applied Physics **100** (2006).

78. J. Adam, G. Klein and T. Lehnert, *Hydroxyl content of $BaTiO_3$ nanoparticles with varied size*, Journal American Ceramics Society **96**, pp. 2987–2993 (2013).

79. T. Noma, S. Wada, M. Yano and T. Suzuki , *Analysis of lattice vibration in fine particles of barium titanate single crystal including the lattice hydroxyl group*, Journal Applied Physics **80**, pp. 5223–5233 (1996).

80. K. Uchino, E. Sadanaga and T. Hirose, *Dependence of the crystal structure on particle size in barium titanate* J. Am. Ceram. Soc. 72 1555–8 (1989).

81. T. Yan, Z.G. Shen, W.W. Zhang and J.F. Chen, *Size dependence on the ferroelectric transition of nanosized $BaTiO_3$ particles*, Material Chemistry and Physics **98**, pp. 450–455 (2006).

82. W. Sun, Size *effect in barium titanate powders synthesized by different hydrothermal methods*, Journal of Applied Physics **100** (2006).

83. S.D. Cho, S.Y. Lee, J.G. Hyun and K.W. Paik, *Comparison of theoretical predictions and experimental values of the dielectric constant of epoxy/$BaTiO_3$ composite embedded capacitor films*, Journal of Material Science: Materials in Electronics **16,** pp. 77–84 (2005).

84. T. Furukawa, K. Fujino and E. Fukada, *Electromechanical properties in the composites of epoxy resin and PZT ceramics*, Journal of Applied Physics **15**, pp. 2119–2129 (1976).

85. T. Hoshina, *Size Effect Of Barium Titanate: Fine Particles And Ceramics*, Journal of the Ceramic Society of Japan **121**, pp. 156-161 (2013).

86. T. Hoshina, H. Yasuno, S.M. Nam, H. Kakemoto, T. Tsurumi and S. Wada, Transactions of the materials research society of japan **29**, pp. 1207-1210 (2004).

87. S. Wada, T. Hoshina, H. Yasuno, S.M. Nam, H. Kakemoto, T. Tsurumi and M. Yashima, Journal of Korean Physics Society **46**, pp. 303-307 (2005).

88. M. Yashima, T. Hoshina, D. Ishimura, S. Kobayashi, W. Nakamura, T. Tsurumi and S. Wada, Journal of Applied Physics **98** (2005).

89. P. Sedykh and D. Michel, Physical Review B **79** (2009).

90. L. Curecheriu, M. T. Buscaglia, V. Buscaglia, Z. Zhao and L. Mitoseriu, Applied Physics Letter **97** (2010).

91. S. Wada, *Preparation Of Nm-Sized Barium Titanate Fine Particles And Their Powder Dielectric Properties*, Japanese Journal of Applied Physics **42**, pp. 6188-6195 (2003).

92. J. Adam, *Ferroelectric Properties Of Composites Containing $BaTio_3$ Nanoparticles Of Various Sizes,* Nanotechnology **25** (2014).

93. T. Lehnert, J. Adam and M. Veith*, Ferroelectric characterization of nondensified particle-based structures*, Journal of Applied Physics **106** (2009).

94. J.W. Silwa, J.S. Ayter, and Mohr, *Method for making piezoelectric composite*, U.S. Patent **5** (1993).

95. S. Livneh, V. Janas, and A. Safari, *Development of fine scale PZT ceramic fiber/polymer shell composite transducer*, Journal of American Ceramics Society **78** (1995).

96. H. Khanbareh, S. van der Zwaag, and W. A. Groen, *Effect of dielectrophoretic structuring on piezoelectric and pyroelectric properties of lead titanate-epoxy composites*, Smart Materials and Structures **23**, p. 105030 (2014).

97. N.T. Mascarenhas, *Highly Flexible Lead-free Piezoelectric Composites*, MSc Thesis, Delft University of Technology (2015).

98. V. L. Stuber, *Lead-free Piezoelectric Composites for Energy Harvesting Applications*, Master's thesis, Delft University of Technology (2017).